# Fracture distribution along open folds in southern Tunisia implications for naturally fractured reservoirs

Smith, Ruaridh Y.; Bruna, Pierre-Olivier; Nasri, Ahmed; Bertotti, Giovanni

**DOI**
10.1144/petgeo2023-039

**Publication date**
2024

**Document Version**
Final published version

**Published in**
Petroleum Geoscience

**Citation (APA)**
Smith, R. Y., Bruna, P.-O., Nasri, A., & Bertotti, G. (2024). Fracture distribution along open folds in southern Tunisia: implications for naturally fractured reservoirs. *Petroleum Geoscience*, *30*(1), Article petgeo2023-039. https://doi.org/10.1144/petgeo2023-039

Research article

PG
*Petroleum Geoscience*

https://doi.org/10.1144/petgeo2023-039 | Vol. 30 | 2023 | petgeo2023-039

# Fracture distribution along open folds in southern Tunisia: implications for naturally fractured reservoirs

**Ruaridh Y. Smith[1*], Pierre-Olivier Bruna[1], Ahmed Nasri[2] and Giovanni Bertotti[1]**

[1] Department of Geoscience & Engineering, Delft University of Technology, Stevinweg 1, 2628 CN Delft, The Netherlands
[2] Mazarine-Energy Tunisia, Rue de la Bourse, Zenith Building, 1053 Tunis, Tunisia
RYS, 0000-0001-8575-7341; P-OB, 0000-0001-9403-8955; GB, 0000-0002-7368-4867
* Correspondence: ruaridh.smith@fau.de
Present addresses: RYS, Geozentrum Nordbayern, Friedrich-Alexander Universität Erlangen-Nürnberg, Schlossgarten 5, 91054 Erlangen, Germany

**Abstract:** Fracture networks play a critical role in fluid flow within reservoirs, and it is therefore important to understand the interactions and influences of these networks. Our study focuses on the Southern Chotts–Jeffara Basin, which hosts reservoirs within Triassic, Permian and Ordovician units containing significant hydrocarbon accumulations. Recent developments on the structural understanding of the basin have proved that a regional shortening phase occurred between the Permian and Jurassic, forming open folds and a distributed fracture network. Analysis of late Paleozoic and Mesozoic outcrops within the basin has identified several sets of fractures (with dip directions and dip angles of 150/80 and 212/86) and compressional structural features that support this shortening hypothesis. We have integrated fracture data from surface analogues and subsurface analysis of advanced seismic attributes and well data through structural linking to form a 2D hybrid fracture model of the reservoirs in the region. Through analytical aperture modelling and numerical simulation, we found that the fractures orientated 212° in combination with large-scale fractures contribute significantly to the fluid-flow orientation and potential reservoir permeability. Our presented fracture workflow and framework provide an insight into network characterization within naturally fractured reservoirs of Tunisia, and how certain structures form fluid pathways that influence flow and production.

**Supplementary material:** Data and figures detailing fracture characterisation and modelling along open folds in southern Tunisia are available at https://doi.org/10.6084/m9.figshare.c.6904499

**Received** 5 April 2023; **revised** 24 October 2023; **accepted** 26 October 2023

The Southern Chotts–Jeffara Basin, southern Tunisia (Fig. 1) is a proven prolific region for petroleum production with significant hydrocarbon accumulations within the Paleozoic and Early Mesozoic reservoirs (Mejri *et al.* 2006; Bruna *et al.* 2019*a*). In these reservoirs, the presence of natural fractures and their role on fluid flow has been largely overlooked. However, it is well known that when reservoir quality is poor (low porosity and permeability), natural fractures represent the only pathways for fluids in the subsurface. It is therefore essential to predict the geometrical organization and properties of natural fracture networks at depth in order to drive successful exploration and to optimize current production (Richard *et al.* 2022).

## Importance of fractures in the Southern Chotts–Jeffara Basin

The Southern Chotts–Jeffara Basin is situated in the Saharan Domain, which is bounded to the north by the deformed Atlassic Chain (Burollet 1991; Fekirine and Abdallah 1998; Galeazzi *et al.* 2010; Soua 2014; Gharbi *et al.* 2015). The Saharan Domain records a Paleozoic and Mesozoic sedimentary series separated by major unconformities. In this domain, several reservoir units have been described (Mejri *et al.* 2006; Balti *et al.* 2018; Bruna *et al.* 2019*a*).

The main reservoirs in the basin are primarily composed of quartzite (Ordovician), carbonates (Permian) and sandstones (Triassic Trias Argilo-Gréseux Inférieur (TAGI)), with the current oil initially in place estimated at 445 MMbbl (Serinus Energy 2022). Both the Ordovician and Permian reservoirs contain low-permeability (<1 mD) and poor matrix porosity but host significant resources (Balti *et al.* 2018), and are classified as naturally fractured (RPS Energy 2018; Kraouia *et al.* 2019). In these petroleum systems, the natural fracture networks play an important role in enhancing flow transmissibility. While essential for exploitation, the presence of natural fractures substantially influences the behaviour of the system. Therefore, predicting the organization and the flow efficiency of the fractures in place is an essential task.

## Challenges linked with naturally fractured reservoirs and first-order solutions

Fractures are multiscale features that promote high-permeability drainage when well connected (Nelson 2001). Conversely, these features can inhibit flow owing to compartmentalization and sealed barriers, causing production issues and inducing unexpected hazards that affect the economic model of resource exploitation (Laubach and Ward 2006; Bourbiaux 2010). Fractures are organized in networks that occur from the microscale to the kilometre scale and interactions between these features can complement the overall network (Bonnet *et al.* 2001; Zhang *et al.* 2016; Bruna *et al.* 2019*c*). Disconnected large-scale fractures can be connected through small-scale efficient networks, and thus it is crucial to understand the dependencies between scales in naturally fractured reservoirs (e.g. Nelson 2001; Darcel *et al.* 2003; Toublanc *et al.* 2005; Boersma *et al.* 2021).

The prediction of natural fracture network geometries and flow properties in reservoirs is a difficult task. Indeed, these networks occur mainly below the resolution of seismic data and hence are quasi-invisible in the subsurface. Boreholes offer the only direct information about the characteristics of the fracture network in the reservoir. Unfortunately, the dimensions of the borehole information (1D) is insufficient to make reliable predictions on what the network would look like at the inter-well to reservoir scales (Wu and Pollard 2002; Maerten *et al.* 2016).

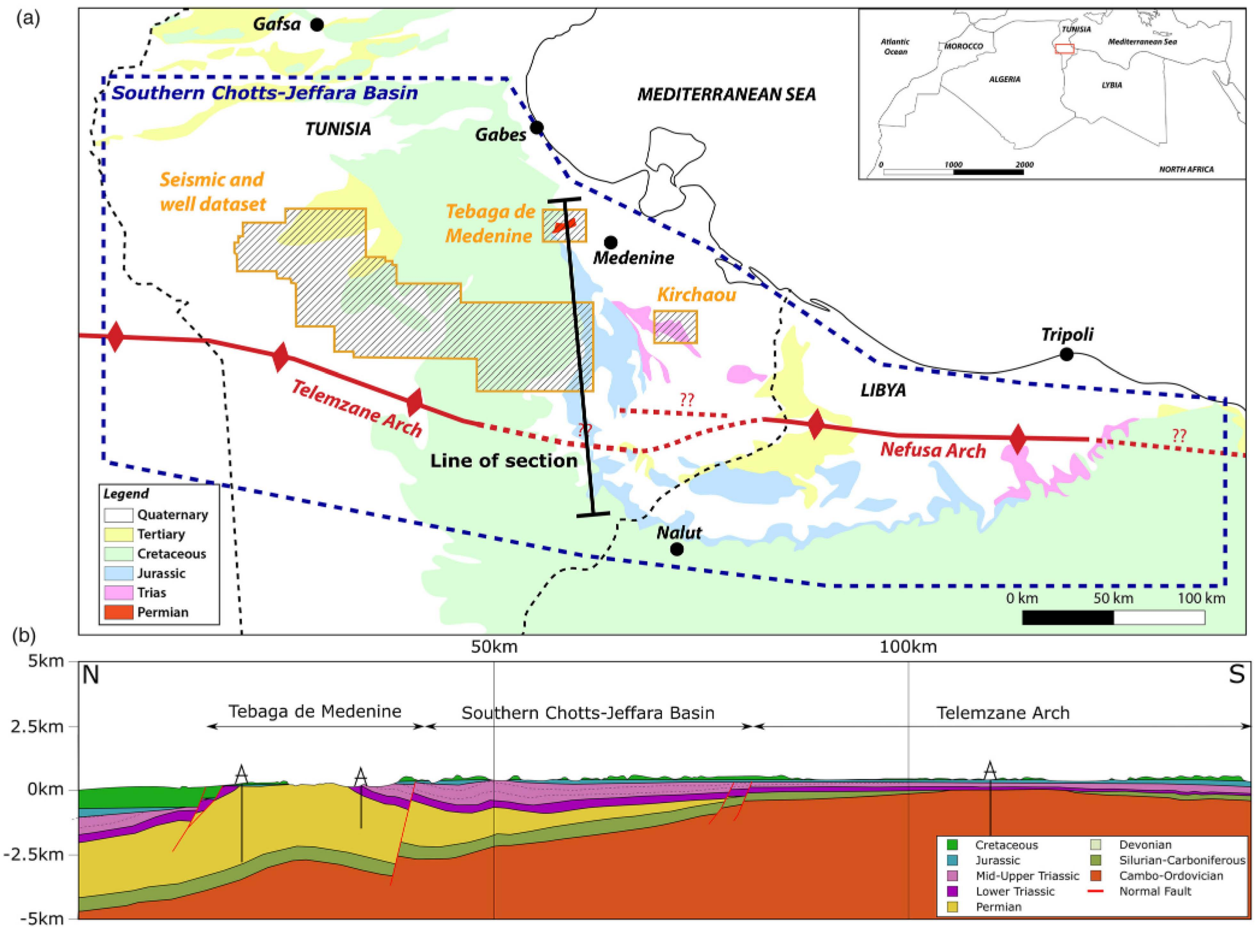


**Fig. 1.** (**a**) The location of interest in central Tunisia showing the Southern Chotts–Jeffara Basin and the main structural features. The map shows areas of: (1) surface study (Tebaga of Medenine and Kirchaou); and (2) subsurface study (seismic and well datasets). (**b**) North–south cross-section through the Tebaga of Medenine and the Telemzane Arch showing the effects of the arch on the distribution of sedimentary series in the Southern Chotts–Jeffara and Ghadames basins (Smith 2020).

Modern advances in seismic processing (e.g. seismic attributes: Boersma *et al.* 2021) have allowed seismic data to be used to image larger fracture and fault networks in the subsurface (Jaglan *et al.* 2015). However, the applicability of these new techniques are limited when constraining smaller fractures at scales of less than the seismic resolution, which remains a challenge (Kattenhorn and Pollard 2001; Lei *et al.* 2017).

The most common and cheaper (compared to core acquisition) method for fracture interpretation lies in the use of wellbore image logs (e.g. Formation Micro Imager (FMI) logs). The use of these image logs proves to be a powerful tool to quickly obtain a representation of the potential impact of fractures at depth. Image logs can come with limitations such as overlooking smaller fractures along the well (Genter *et al.* 1997; Wu and Pollard 2002; Khoshbakht *et al.* 2012). In addition, the geometry of the fractures can only be partially retrieved from the wellbore images. Fractures may be longer or more widely spaced than the wellbore diameter, which leads to poor sampling and an underestimation of the network complexity (i.e. fractures parallel to the well trajectory tend to be underrepresented: Terzaghi 1965; Belfield and Sovich 1995; Ortega *et al.* 2006 and references therein).

## Use of surface analogues to reduce uncertainties in reservoir fracture modelling

The availability of outcrops surrounding the targeted reservoirs is an asset to complement the data available from the subsurface. The eastern part of the Southern Chotts–Jeffara Basin presents such an advantage. In the Jeffara Escarpment and the Tebaga of Medenine a series of outcrops (Permian–Mesozoic in age) are accessible. Direct observations of fracture networks at various scales can be interpreted with the partial information retrieved from wells and seismic data (Stephenson *et al.* 2007; Welch *et al.* 2015).

The prerequisite to use outcrop data to better understand the subsurface is to establish the analogy between the two domains. Several important factors influence the establishment of the link between outcrop and subsurface. The most influencing parameters are: (i) the degree of alteration of the outcrop (Li *et al.* 2018) compared to the reservoirs – weathering leads to alteration, which affects the rock properties in the outcrop compared to the subsurface; (ii) the shared geological history between the two domains and, more importantly, the shared tectonic events responsible for the emplacement of fractures (presence or not of tectonic drivers); and (iii) a comparable rock type between the outcrop and the subsurface. A shared tectonic history can be interpreted through establishing which tectonic drivers are affecting local and regional stress regimes, such as the influence of faults on localized fractures (e.g. Micarelli *et al.* 2006; Mitchell and Faulkner 2009; Maerten *et al.* 2016), the development of large-scale fracture networks within folded regions (Zahn and Hennings 2009; Watkins *et al.* 2018), and burial-related fracturing from regional vertical and far-field stresses at a tectonic scale (Lamarche *et al.* 2012; Lavenu *et al.* 2013; Bisdom *et al.* 2016*a*). Furthermore, observing fracture networks in multiple outcrops spread across a sufficient area (>10 km) allow the geometrical regularity of a network to be quantified and, hence, analogue uncertainty to be reduced.

When the analogy is established, outcrops can provide some key missing information compared to the subsurface. For instance, fracture length and geometrical variability, typically inaccessible from borehole data, can be obtained from outcrop pavements (i.e. $x$ and $y$ orientated outcrops). The retrieved information can be transposed as statistical rules in the subsurface domain to drive a more accurate network prediction (Gutmanis *et al.* 2018).

### Static and dynamic modelling of naturally fractured reservoirs

Discrete fracture network (DFN) stochastic modelling, driven by specific fracture parameters (e.g. orientation distribution, length and intensity), is the most common method used to predict fractures within the subsurface (Cacas *et al.* 2001; Chilès 2005; Bisdom *et al.* 2014; Huang *et al.* 2017; Bruna *et al.* 2019*c*; Loza Espejel *et al.* 2020).

However, this modelling technique has its limitations. The consideration of statistic distributions to approximate the geometry of the modelled network leads generally to a poor matching of the fracture model with the conditioning data (e.g. well data). In addition, the uncertainties at the inter-well distance remain a major challenge that DFN stochastic modelling studies are rarely addressing. Recent alternatives aimed at improving the geological robustness of fracture network models have been proposed. For example, work by Chugunova *et al.* (2017) and by Bruna *et al.* (2019*c*) have used multiple point statistics to generate fracture network models. This method offers the required flexibility to integrate geological information early in the modelling process and, hence, improve the consideration of discrete information at the borehole location. However, limitations remain on the use of images to generate discrete objects (i.e. fractures). Concerning the inter-well distance, recent studies (i.e. Boersma *et al.* 2021) have used unconventional seismic attributes to image first-order fractures that can be integrated with smaller-scale DFN models.

DFN solvers generate static models that respect the characteristics of fracture networks obtained from surface and subsurface data. These models require validation through dynamic data and modelling. There are several methods and solvers to simulate fluid flow through fracture networks, such as ABAQUS (e.g. Cruz *et al.* 2019), COMSOL Multiphysics (e.g. Lepillier *et al.* 2019; Stoll *et al.* 2019) and MOOSE Framework (e.g. Grimm Lima *et al.* 2020; Poulet *et al.* 2021; Smith *et al.* 2022). One of the challenges associated with simulating fluid flow through fractured media lies with the estimation and integration of the fracture aperture, which is generally linked with permeability and can be computationally expensive. Methods treating fractures within the network mesh as flat features (lower dimensional elements), where the fracture aperture is applied numerically, has enabled more efficient simulations of fracture fluid flow and permeability (Cacace and Jacquey 2017; Poulet *et al.* 2021; Smith *et al.* 2022). It seems that a best practice for modelling complex fracture networks lies with a coupled approach integrating multiscale fracture network models and fluid-flow simulations that account for dynamic apertures to better represent and model the subsurface.

### Objectives of this research

In this paper we investigate the fracture networks present in the Southern Chotts–Jeffara Basin in southern Tunisia (Fig. 1). Whilst several studies have focused on the sedimentology and reservoir properties of the units in the basin (e.g. Galeazzi *et al.* 2010; Soua 2014; Jabir *et al.* 2020), there has been limited work on the fracture networks and their effects on fluid flow. Production data from the region of interest in the Southern Chotts–Jeffara Basin has indicated that fractures are contributing to dual-porosity behaviour. However, this flow behaviour has yet to be quantified or integrated in multiscale models (RPS Energy 2018; Serinus Energy 2022).

We propose a workflow where small fractures are modelled using stochastic techniques (e.g. DFN modelling) with data acquired from outcrops (e.g. fractured pavements) and wells (e.g. FMI logs). To integrate large-scale fractures within the model, unconventional seismic processing attributes that detect linear structural anomalies are used to deterministically trace larger fractures in reservoirs (Jaglan *et al.* 2015; Boersma *et al.* 2021). These two sources of data result in a multiscale fracture realization from which additional fracture properties (aperture and permeability) can be analytically and numerically determined and simulated.

## Case study: Southern Chotts–Jeffara Basin

### Present-day setting in central Tunisia

The Southern Chotts–Jeffara Basin (Fig. 1) is situated within the Saharan structural domain and adjacent to the Atlassic Domain boundary in the north (Soua 2014; Bruna *et al.* 2019*a*; Jabir *et al.* 2020). The Saharan Domain forms the foreland to the Atlassic Domain and is generally considered to be stable and poorly deformed (Fekirine and Abdallah 1998; Bouaziz *et al.* 2002).

One of the prominent features within the region is the Paleozoic Telemzane Arch, an east–west-trending anticline (Fig. 1) observed in the subsurface through gravity anomalies (Dhaoui *et al.* 2014; Troudi *et al.* 2018), seismic data and wells (e.g. OS-1: Mejri *et al.* 2006; Soua 2014). During various Paleozoic orogenic events, movements along the arch have caused the removal or non-deposition of several series from the Silurian to the Permian; however, the history of the arch is complex and still debated, and falls beyond the scope of this paper (Bouaziz *et al.* 2002; Lavier and Buck 2002; Soua 2014).

The basin offers two distinct domains where stratigraphic units are preserved. Towards the west, a Cambrian–Mesozoic series is preserved in the subsurface and is accessible through wells and seismic data (Soua 2014; Bruna *et al.* 2019*a*; Gharsalli and Bédir 2020). This is interrupted by major angular unconformities related to regional erosional processes (Soua 2014). Two principle angular unconformities are visible in the western part of the basin: one occurring at the top of the Carboniferous, and another occurring at the interface between the Permian and the Triassic (Raulin *et al.* 2011; Soua 2014; Bruna *et al.* 2022*b*).

Towards the east, a unique (at the scale of North Africa) succession of Upper Permian marine deposits crop out (Fig. 2a) in the Tebaga of Medenine (Raulin *et al.* 2011; Zaafouri *et al.* 2017; Jabir *et al.* 2020). This outcrop is key as it provides an excellent insight into the regional geological history of the late Paleozoic. The Tebaga of Medenine forms an east–west-trending structure formed of dipping Permian and early Triassic units capped unconformably by younger Mesozoic sediments. The Mesozoic series crops out along the escarpment and in the Jebel Rehach area (Kirchaou: Fig. 2b). The preserved series is about 2500 m thick and dips gently (2°–3°) towards the west. The succession is composed of clastic, carbonate and evaporitic deposits (Lazzez *et al.* 2008; Galeazzi *et al.* 2010; Jabir *et al.* 2020).

### Structural history of the Southern Chotts–Jeffara Basin

Prior to the Carboniferous, the basin underwent a series of complex tectonic phases primarily controlled by extensional and strike-slip regimes establishing highs and lows (Caledonian and Taconian orogenies). These tectonic phases are marked by a series of

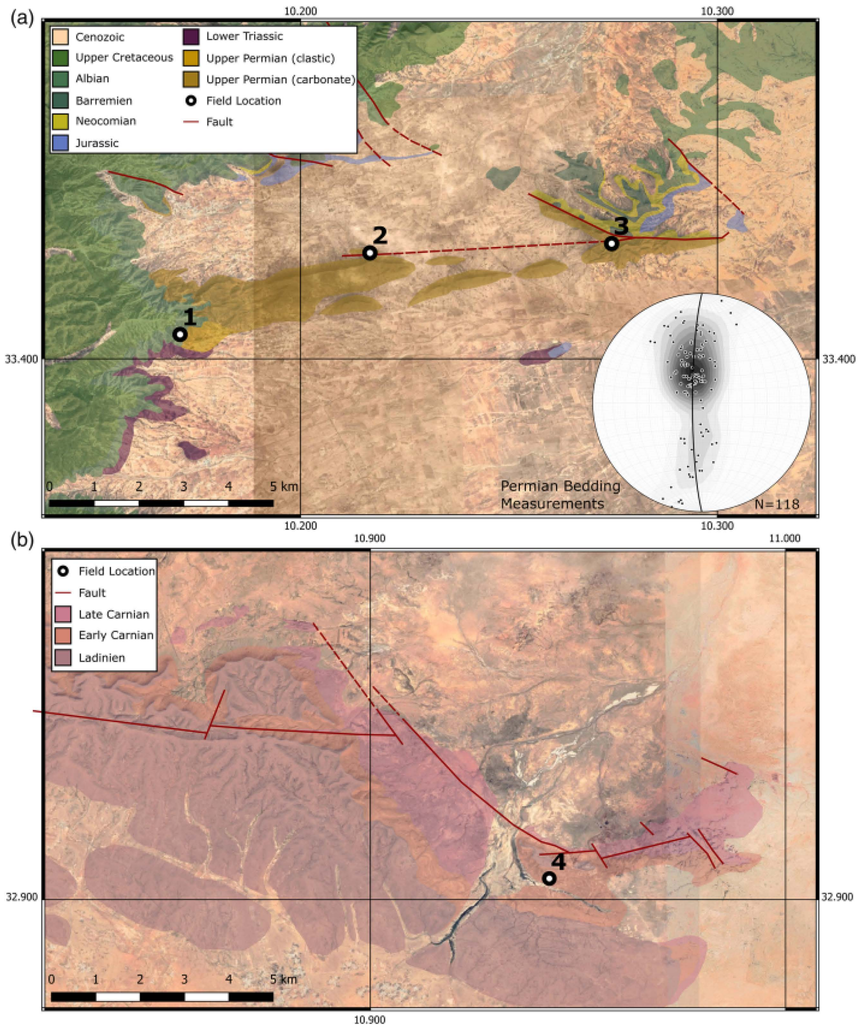


**Fig. 2.** Geological maps showing the location of field data collection points (fracture measurements and pavement imagery) in (**a**) The Tebaga of Medenine (inset: stereoplot (Schmidt projection of Permian bedding showing a north–south fold axis)) and (**b**) Kirchaou (modified from Bouaziz and Ben Salem 1987; Bouaziz and M'Hadhbi 1987; Zouari *et al.* 1987).

unconformities (Mejri *et al.* 2006; Soua 2014; Bruna *et al.* 2019*a*; Reeh *et al.* 2019). The Hercynian Orogeny initiated during the Carboniferous (Stampfli and Borel 2002; Frizon de Lamotte *et al.* 2013), affecting the entire region through the reactivation of faults, block tilting and folding. Deformation associated with the Hercynian Orogeny is truncated by a series of major diachronous unconformities found within the Paleozoic series (e.g. Frizon de Lamotte *et al.* 2013).

The period between the late Permian and the Cretaceous has been subject to several studies presenting differing hypotheses as to the structural nature and evolution of the basin and the Tebaga of Medenine (Mathieu 1949; Bouaziz *et al.* 2002; Stampfli and Borel 2002; Raulin *et al.* 2011; Bruna *et al.* 2020; Smith 2020). These studies focus on characterizing a major angular unconformity between the early Triassic and Jurassic units. Early studies suggested a shortening phase prior to the Jurassic that caused reverse faulting and folding along the east–west-orientated structure (Mathieu 1949). Bouaziz (1995) and Bouaziz *et al.* (2002) proposed that transcurrent faulting formed an asymmetrical anticline during the late Triassic, based on field evidence of the structure. Raulin *et al.* (2011) alternatively argued that extension along previous east–west-trending major faults caused block tilting and uplift of the Tebaga of Medenine. A recent study proposed that the region underwent a period of persistent shortening from the early Triassic to the Jurassic based on field, seismic, borehole and thermochronological data, causing localized intense compressive deformation and major vertical uplift movement in the basin (Bruna *et al.* 2020; Smith 2020). This uplift and shortening formed the Tebaga of Medenine and subsequently another regional anticline orientated NW–SE in the Jeffara Plain (Smith 2020; Bruna *et al.* 2022*b*).

After a general phase of subsidence in the area of interest, the Alpine phase was initiated during late Cretaceous and persisted until the late Eocene. Whilst the impact of this phase in the Southern Chotts–Jeffara Basin remains very limited, gentle anticlines and associated unconformities have been observed in the Chotts ranges to the north (Bodin *et al.* 2010; Saïd *et al.* 2011).

## Linking the surface to the subsurface: a regional shortening at the beginning of the Triassic

The Permian and Triassic sedimentary units observed in outcrop are direct analogues where the same formations are present at depth in the western Southern Chotts–Jeffara Basin and have experienced similar structural histories (Bruna *et al.* 2019*a*, 2022*b*; Smith 2020). Therefore, the data collected from the outcrops complement the data interpreted from the subsurface.

In the Tebaga of Medenine and Kirchaou, the observed regional-scale structural features (folding of the Tebaga of Medenine and reverse faulting generating antiformal stacks) support the model of Smith (2020) and Bruna *et al.* (2022*b*), and indicate a period of shortening in the region affecting the Permian–early Jurassic units. This shortening phase is directed north–south and forms large open folds in the basin. The widespread distribution of folds across the basin implies their potential role as a driver of inelastic deformation (i.e. fracture formation during the layer-parallel shortening phase). This major shortening event equally deforms older underlying units (Smith 2020; Bruna *et al.* 2022*b*). The working hypothesis proposes that the fracturing pattern in older rock compares to the patterns observed in the Tebaga of Medenine as it is generated by the same event and driven by the same structural elements (folds).

We can link the surface structural interpretations to the subsurface in the western section of the basin through the presence of large-scale open folds (Fig. 3). A structural high (Matmatah Arch) that corresponds to a similar timing and fold-axis orientation as the Tebaga of Medenine is observed in seismic to the west of the Tebaga of Medenine and has caused identical thinning of the Mid–Late Triassic units (Ben Ferjani *et al.* 1990). Palinspastic restorations of the basin based on regional seismic lines (>700 km of data) also indicate the possible presence of a subsurface palaeohigh extending from the Jeffara Escarpment towards the west and affecting the underlying reservoirs (Bruna *et al.* 2019*a*). The presence of this fold in the basin implies the units at depth in this area have undergone a similar deformation history as the surface units. Therefore, the surface fractures related to the shortening event can be predicted to occur at depth within the Triassic and Paleozoic reservoirs, and can be used as the basis for modelling fractures at depth. As fractures at the large scale present generally similar characteristics as smaller-scale fractures (Ortega *et al.* 2006; Boersma *et al.* 2018), the analysis of fracture attributes in seismic data is key as it represents a benchmarking element in validating the modelled geometry.

## Methodology and data integration

### Surface data acquisition

Surface fracture data was obtained from Permian–Cretaceous outcrops (Fig. 2) located along the Jeffara Escarpment (Triassic–Cretaceous), Tebaga of Medenine (Fig. 2a: Late Permian and Early Triassic) and Kirchaou (Fig. 2b: Mid–Late Triassic). Measurements were taken throughout the Tebaga of Medenine, with an emphasis given to the characterization of the fold axis and limbs of this structure. The goal was to acquire a spatially widespread dataset across the structure and so enable analysis of the fracture distribution. Fracture measurements were made throughout the Tebaga of Medenine and along the limbs of the fold structure, and were corrected for folding orientation to limit sampling biases. In addition to fracture measurements collected around the structure, three fractured pavements from the Tebaga of Medenine and Kirchaou were imaged (metre scale) to gather additional 2D datasets that would provide statistical data to characterize the fracture networks. Pavement locations were based on the quality of exposure along the fold and the spatial variability from the main structure. The imaging process involved mounting a camera onto an extendable stick to capture multiple images, which were then combined using the photogrammetric principle of triangulation to create a set of orthorectified images from which 2D fracture analysis could be undertaken using the FracPaQ program software (Healy *et al.* 2017). This analysis included determining fracture intensity, an important component of geometrical predictions and one that is difficult to measure from subsurface data (i.e. wells only provide 1D information, $P_{10}$, number of fractures per unit length of borehole: Dershowitz and Herda 1992). Correlating these measurements to a $P_{32}$ volumetric discontinuity intensity value (area of fracture per unit volume) can be problematic across dimensions and thus the use of surface pavement analogues to calculate $P_{21}$ (length of fracture per unit area) provides an intermediate fracture dimensioning that allows a more accurate estimate of the $P_{32}$ intensity (Bisdom *et al.* 2014; Healy *et al.* 2017). Fracture connectivity is an additional important controlling parameter to fluid flow that can be determined from pavement analysis using topological relationships. The *X*–*Y*–*I* node connections or the number of connections per line with certain thresholds ($C_L$: generally between 1.5 and 3.5) defines the quality of percolation and indicates the effectiveness of the fracture network for fluid flow (Balberg *et al.* 1984; Manzocchi 2002; Sanderson and Nixon 2015).

### Subsurface data acquisition

Subsurface data was obtained from wells and 3D seismic situated in the western part of the Southern Chotts–Jeffara Basin where targeted reservoirs appear at depth. FMI data from the wells were used to pick fractures that intersect the borehole. Fracture characteristics (e.g. orientation, azimuth, 1D intensity and corrected $P_{10}$ intensity using the Terzaghi 1965 method) were calculated using Techlog® software. A strict sampling method was applied to remove drilling-induced fractures to ensure that only natural fractures were identified. In general, across both wells the fractures were open and unfilled.

In addition to well data, 3D seismic data are available for the target reservoirs. There are various conventional seismic attributes (e.g. similarity and curvature) that can highlight structural features (e.g. Brown 2001; Chopra and Marfurt 2007). We used a recently developed workflow from OpendTect® that allowed us to compute unconventional attributes (e.g. fault likelihood and thinned fault likelihood) from 3D seismic cubes, and to detect and highlight fractures more effectively (Brouwer and Huck 2011; Jaglan *et al.*

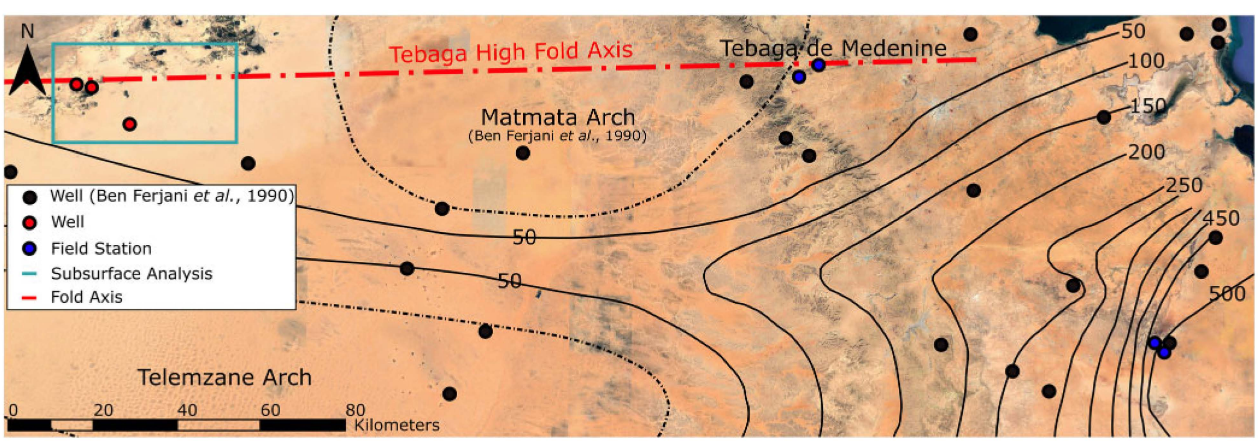


**Fig. 3.** Isopach map showing thinning of the Middle Triassic towards the Matmata Arch (subsurface western extension of the Tebaga of Medenine) and showing the structural link between the surface and subsurface data in the Southern Chotts–Jeffara Basin. Map modified after Ben Ferjani *et al.* (1990).

2015; Boersma *et al.* 2021). The workflow (Fig. 4) proposed by Jaglan *et al.* (2015) applies three main steps of filtering to a seismic steering cube to emphasize structural dip trends and to condition the data for fault and fracture detection:

(1) conditioning and smoothing of the data through dip-steered median filtering (DSMF);
(2) enhancement of fault and fracture lineations through dip-steered diffusion filtering (DSDF); and
(3) combining steps (1) and (2) to create a structurally enhanced seismic steered cube through fault enhancement filtering (FEF).

DSMF (Fig. 4c) is a filter that smooths the seismic volume and removes background noise, therefore improving the continuity of seismic reflectors. This filter is used in conjunction with other filters (e.g. DSDF) as small fault zones may be filtered out by the median filter size. DSDF (Fig. 4d) increases the sharpness of the fault zones by replacing the central amplitude of reflectors with better quality nearby amplitudes. In the proximity of faults and fault zones, the strong seismic reflectors highlight the fault edges and thus sharpen the fault plane (Brouwer and Huck 2011; Jaglan *et al.* 2015). The outputs of these two filters are combined into the FEF (Fig. 4e), which enhances the fault and fracture zones within the seismic for use in alternative attribute processes such as ridge enhancement filtering, providing a more robust image of faults in the subsurface than conventional filters.

Fault likelihood (FL) (Fig. 4g) and thinned fault likelihood (TFL) (Fig. 4h) seismic attributes are calculated from the FEF and are defined by the power of semblance. The FL attribute highlights areas where structural lineations occur and the TFL applies an output in a ratio of 0 (no semblance) to 1 (high semblance), identifying faults and fractures in the reflectors. These attributes also highlight the zones of increased fracture density in the subsurface: that is, where the ratio is larger, more lineations are predicted to be present. Using these attributes, 2D fractures can be traced and analysed, providing data on large-scale fractures in the basin.

### Fracture data integration and modelling workflow

The fracture data acquired from outcrops, seismic and wells were used as input for modelling fracture networks at depth in the Southern Chotts–Jeffara Basin using a fracture modelling approach (Fig. 5) that culminates in the numerical simulation of fracture network fluid flow. Small-scale (metre-scale) fracture data and parameters from outcrops (e.g. orientation, intensity and length) and from wells (orientation, intensity) were integrated as statistical distributions into a discrete fracture network model (DFN) to output a stochastic fracture network model of the reservoirs. The large-scale fractures (tens of metres up to kilometres) were captured using the advanced seismic attribute process and discretized into a 2D deterministic fracture model. With no published studies exploring the role of fractures within the central Tunisian reservoirs, we present the first multiscale hybrid fracture model integrating stochastic and deterministic models to represent the fracture connectivity of the Southern Chotts–Jeffara Basin. In this study we applied analytical aperture modelling based on the present-day stress regime interpreted from borehole data to the static fracture model. The mechanically constrained aperture calculation was used to derive and upscale the permeability field for the subsurface reservoir units of the Southern Chotts–Jeffara Basin and to evaluate the impact of this effective permeability property on fluid flow.

## Surface fracture expression in the Southern Chotts–Jeffara Basin

### Fractures observed in outcrops

Fractures were observed in Upper Permian and Triassic units that are primarily formed of carbonates and sandstones. The Permian units situated in the Tebaga of Medenine (Fig. 2a) have a general structural dip of 30° south. However detailed observations within

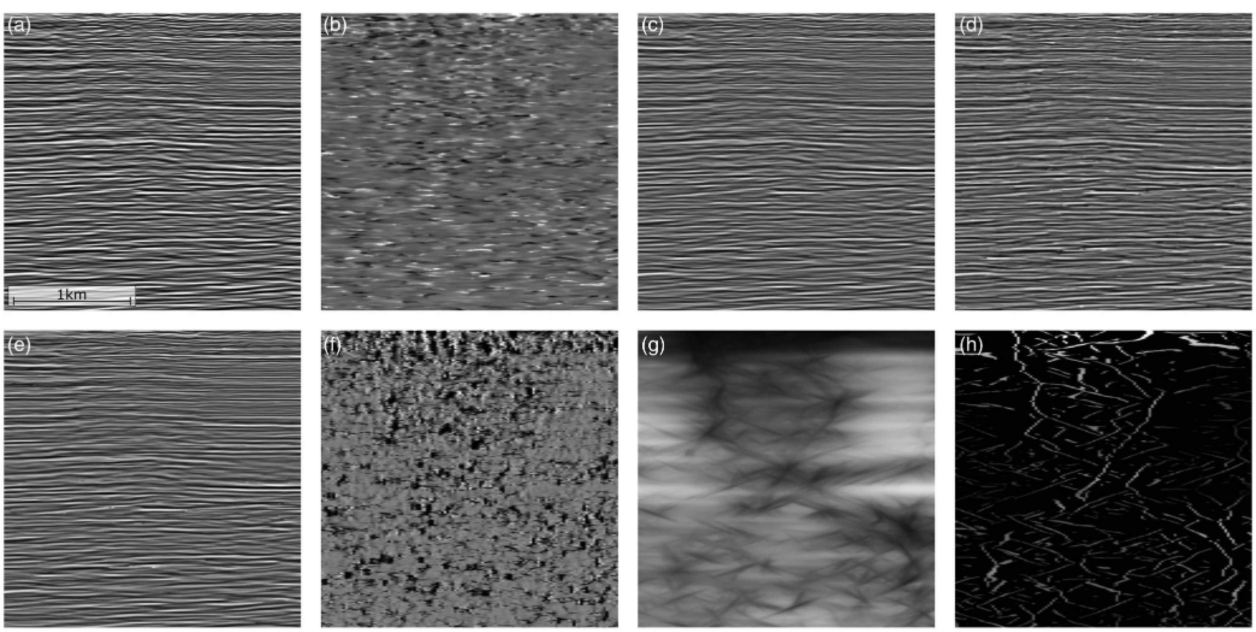


**Fig. 4.** Unconventional seismic attribute workflow to obtain fault and fracture expression in the subsurface: (**a**) initial seismic cube; (**b**) steering cube used for calculating attributes; (**c**) dip-steered median filter (DSMF) removes background noise; (**d**) dip-steered median filter (DSDF) sharpens fault and fracture zones; (**e**) fault enhancement filter (FEF) combines the DSMF and DSDF, providing the base for the fault and fracture attributes; (**f**) ridge enhancement filter highlights the structural lineations within the seismic cube; (**g**) fault likelihood (FL) is calculated from the FEF and the enhanced fracture dense zones; and (**h**) thinned fault likelihood (TFL) sharpens these zones to highlight individual faults and fractures within the seismic.

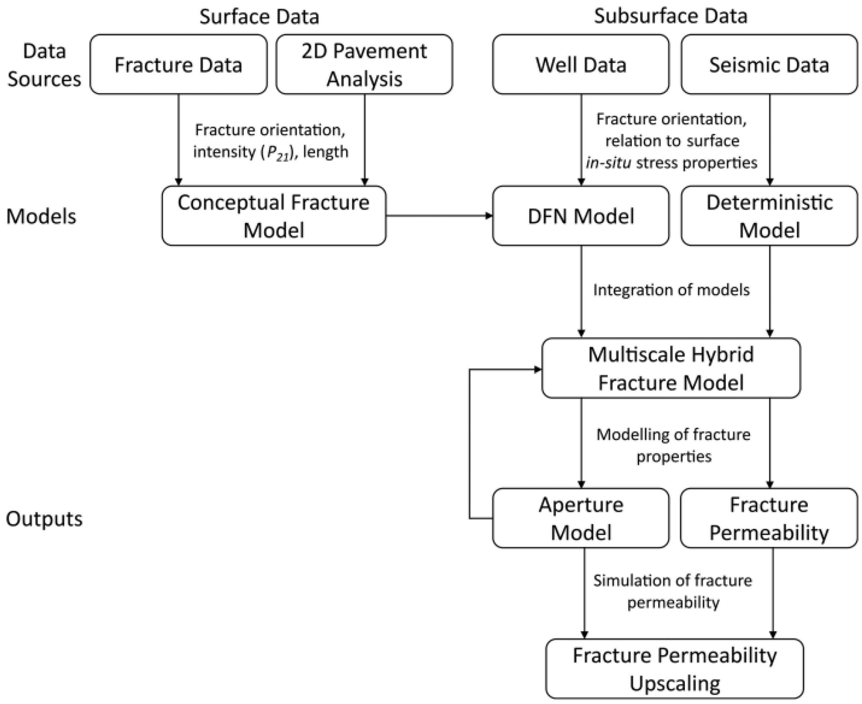


**Fig. 5.** Fracture modelling workflow through the integration surface and subsurface data analysis to create a hybrid fracture model of the Southern Chotts–Jeffara Basin subsurface and to simulate fracture network and fluid-flow properties.

the Tebaga of Medenine showed areas where the dip of these units reached high-angle values towards both north and south dip directions (Fig. 2a, inset). The Lower Triassic sits conformably over the Permian in the Tebaga of Medenine, while the Middle and Upper Triassic are observed unconformably on the Lower Triassic and thicken to the east towards Kirchaou (Fig. 2b).

Fractures and stylolites (Fig. 6) are observed across the region. We observed two main dominant sets of fractures striking approximately 150° and 212° (sets 1 and 2). The acute angle between these fractures is *c*. 60°. In addition, these fractures present an indication of opposite shearing movements (striations), indicating that they are conjugated. From the orientation of the acute angle, the main palaeohorizontal stress ($\sigma_1$) was calculated as 001° (north–south). The fractures in the Tebaga of Medenine (Fig. 7a–c) are primarily open with minimal calcite infill. Whilst the origin of the calcite is outside the remit of this study, the lack of significant weathering of the outcrops indicates that these limited calcite infills are likely to be representative of the maximal mechanical aperture of these fractures in the subsurface. Tectonic stylolites (perpendicular to bedding) were also observed in the Tebaga of Medenine (Fig. 6c) and Kirchaou (green lineations in Fig. 7). The stylolites strike east–west (090°) with the peaks orientated in a north–south direction, indicative of the similar palaeostress ($\sigma_1$) calculated from the conjugate fractures. The stylolites therefore appear to be synchronous with the emplacement of the conjugated system of fractures and therefore formed during the same stress event.

## Fracture pavements

Three fracture pavements were analysed that varied in size from 172–2000 m$^2$. The results of the analysis are presented in Table 1.

Within the three investigated pavements, we found the same conjugated fracture system (sets 1 and 2) as defined by field measurements across the structure (Fig. 2a). In pavements 2 and 3

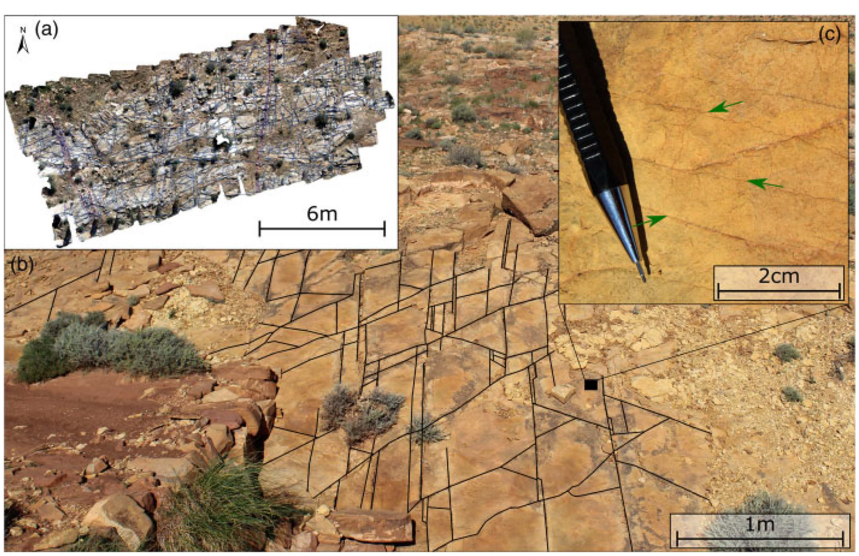


**Fig. 6.** (**a**) Surface fractures observed in the western section of the Tebaga of Medenine within the Permian units. (**b**) Interpreted fractured pavement from the area. (**c**) Stylolites observed within units with north–south-orientated peaks, indicating compressional direction.

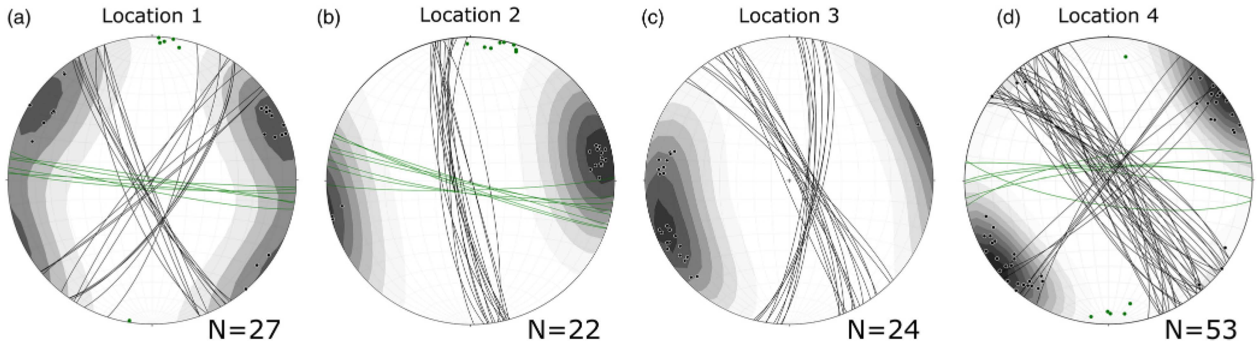


**Fig. 7.** Stereoplots (Schmidt projection) of structural data collected in the field (the location points correspond to Figure 2: (**a**) Tebaga west; (**b**) Tebaga centre; (**c**) Tebaga east and (**d**) Kirchaou. Fractures (black) show a conjugated set (sets 1 and 2) with an acute angle of 60° and stylolites (green) that correspond to a north–south compression orientated 001°.

(Kirchaou area) several shear fractures (echelon and horsetail fractures) orientated predominantly NW–SE and NE–SW were also observed. This localized variability in fracture orientation is due to the presence of strike-slip faults in the area. Average fracture lengths showed similarities between pavements; however, there is variation in the maximum length, possibly due to the different lithologies and carbonate facies present (Whitehead *et al.* 1987; Michie *et al.* 2014).

Connectivity analysis of the fracture networks within the three pavements shows that between 24 and 39% of the fractures are connected through either cross-cutting or abutment relationships and connectivity is within the range of connections per line that satisfies good system percolation (Balberg *et al.* 1984; Manzocchi 2002; Sanderson and Nixon 2015).

General areal fracture intensity ($P_{21}$) was also estimated from the pavement imagery and is *c.* 0.065 m m$^{-2}$. From the areal intensity, the volumetric intensity ($P_{32}$) was initially estimated as 0.063 m$^2$ m$^{-3}$, calculated from correction factors (Dershowitz and Herda 1992; Mauldon and Dershowitz 2000), and that $P_{21} \approx P_{32}$ as a function of the Fisher coefficient ($K < 50$) (Bisdom *et al.* 2014).

## FMI data and seismic attribute fracture detection for subsurface characterization

Subsurface fracture characterization was undertaken using both 3D seismic and FMI well data from the western part of the Southern Chotts–Jeffara Basin providing information at different scales. The FMI provides 1D point data of directly observed fractures at the centimetre scale, whilst the seismic data provide fracture data at the tens of metres to kilometre scale and integrates the scattered well data. Fractures are detected using seismic attribute analysis that captures the long fractures that may not cross the wells. Seismic analysis can also highlight variations in fracture intensity, indicating the flow zones in the reservoirs.

### Fracture interpretation from FMI data

The FMI data of two vertical wells (Well 1 and Well 2) were analysed to interpret the natural fractures. The wells lie within the same structural domain as the outcrops along the large open fold system and are separated by a large subsurface fault. FMI was available for 200 m in each well at similar depths within the same reservoirs. Drilling-induced fractures were discarded from the FMI interpretation by identifying complete sinusoidal features and structures orientated with the borehole.

Three main azimuth orientations (Fig. 8) were identified in the fractures: (1) 240°, (2) 300° and (3) 001°. The general dip sense of all the fractures varied between *c.* 65° and 85°. Sets 1 and 2 (shown in green in Fig. 8) correspond to the conjugate sets (sets 1 and 2) that were observed on outcrops, with a slight variation in orientation that is likely to be due to local *in situ* stresses at depth. The dominant set in the well data is Set 3 (shown in red in Fig. 8: east–west strike), which was not observed as regularly on the surface.

Using the Terzaghi correction to compensate for the orientation and spacing sampling biases in the borehole (Terzaghi 1965), a series of corrected global $P_{10}$ values were calculated for each well. Well 1 and Well 2 showed varying values for the corrected $P_{10}$ fracture intensity. The corrected $P_{10}$ values in Well 1 and Well 2 were calculated as 0.0366 and 0.0905 m$^{-1}$, respectively. The fracture intensity showed some variations through both wells caused by intersections of the borehole with fault and fracture zones.

### Fracture interpretation from 3D seismic data

The 3D seismic survey covers an area of 330 km$^2$ of the western Southern Chotts–Jeffara Basin. However, for a better efficiency in the seismic attribute processing, a smaller area (12.5 km$^2$) in the NW is used for the attribute analysis which covers the location of the wells.

The TFL attributes detected around 1300 lineaments in the seismic cube from which the main orientations (Fig. 9) are a conjugated fracture set (shown in green in Fig. 9) presenting similarities with the conjugate set observed in outcrop and fracture sets striking east–west (Set 3) and north–south (Set 4). The interpreted lineaments observed both in map and section views in the seismic indicate limited movement and can, therefore, be treated as fractures rather than faults. The east–west and north–south sets present the larger fracture sets within the subsurface. The east–west set correlates with the dominant fracture orientation (Set 3) observed

**Table 1.** Fracture pavement analysis results

| Pavement | No. of detected traces | Average trace length (m) | Maximum trace length (m) | Average $P_{21}$ value (m m$^{-2}$) | Connectivity (*Y–X–I*) |
|---|---|---|---|---|---|
| 1 | 902 | 0.725 | 9.175 | 0.065 | 0.10–0.29–0.61 |
| 2 | 1161 | 0.878 | 12.250 | 0.048 | 0.11–0.13–0.76 |
| 3 | 597 | 1.663 | 19.225 | 0.065 | 0.11–0.28–0.61 |

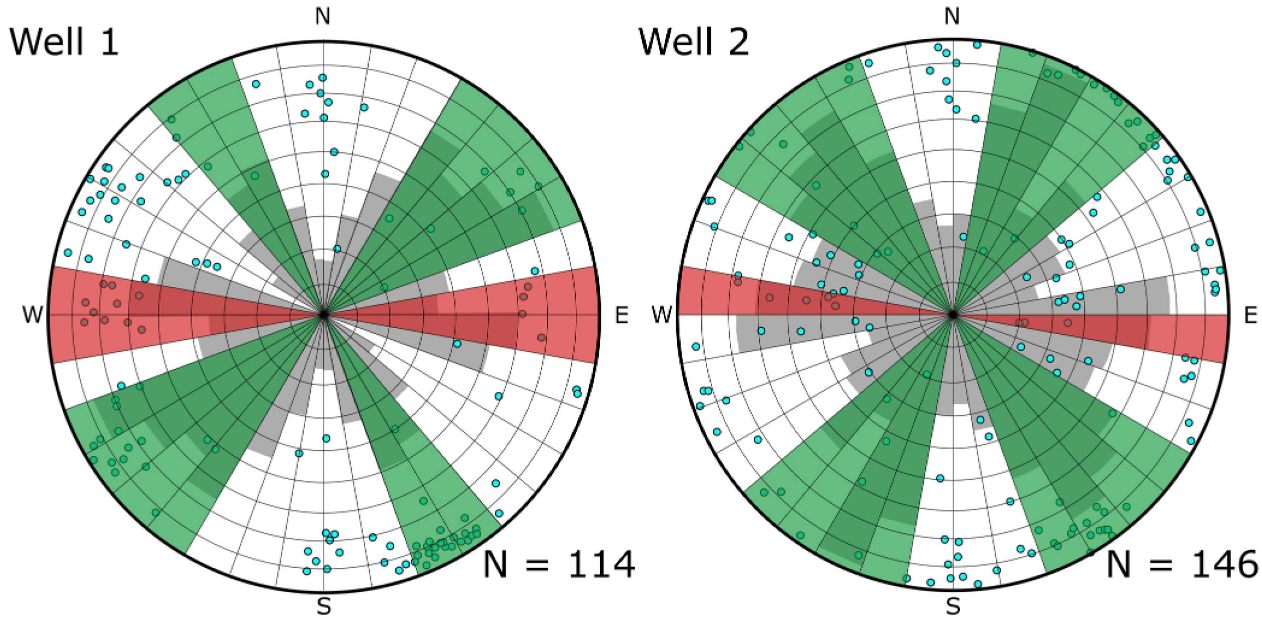


**Fig. 8.** Stereoplot (Schmidt projection) and strike rose diagram showing the observed fractures in the wells located within the Southern Chotts–Jeffara Basin. Conjugate sets (green) correspond to the same sets (sets 1 and 2) observed in the field. An additional set (red: Set 3) is observed that formed prior to the Permian shortening phase.

within the well data and these two additional fracture sets are observed to be distributed throughout the system.

Whilst the TFL does not provide quantifiable data on the fracture intensity, it does indicate the areas where increased areal intensity is present, which correlates to possible flow zones within the reservoirs assuming that constant flow properties are present within the reservoirs. The TFL attribute calculations computed in the area of interest show that Well 1 is located within a region of low fracture density compared to Well 2 where fracture density is higher. This correlates with the global corrected $P_{21}$ values of the wells where there is a higher areal fracture intensity in Well 2 compared to Well 1.

Fracture length can also be analysed from the TFL attribute and varied from 15–200 m, complementing the smaller fracture data from outcrop and wells. Fracture attributes can be characterized accurately across multiple scales and fracture populations of different scales can be related over a scale invariance (Walsh and Watterson 1988; Marrett *et al.* 1999). Therefore, the three structural datasets (outcrop, seismic and well) complement one another to create a complete fracture framework of the reservoirs.

## Integration into the geological framework

The two main fracture sets measured in the Tebaga of Medenine and within the subsurface are the conjugate sets orientated NNE–SSE and NNW–SSE (sets 1 and 2) and formed during a north–south-orientated shortening event dated as Lower Triassic (Smith 2020; Bruna *et al.* 2022*b*). This regional event caused the occurrence of open folds orientated east–west that can be observed in seismic and in the field across the limbs of the Tebaga of Medenine. The widespread distribution of the conjugate fracture sets (Fig. 10) across the folded region is concomitant with the emplacement of these open folds. Conjugate sets observed in the basin are associated with the early compressional stages (layer parallel shortening (LPS)) and the widespread distribution of the fractures occurs due to the brittle behaviour of the rocks, such as the Permian carbonates (e.g. Swanson 1988; Tavani *et al.* 2011; Branellec *et al.* 2015). As this shortening event occurred at the end of the Paleozoic and the beginning of the Mesozoic, the earlier Paleozoic units are also likely to have been affected. This is observed through the identification of these conjugate fractures in the western part of the basin (Fig. 8: Well 1 and Well 2) and in the seismic data (Fig. 9). The identification of the same sets in the subsurface data (Fig. 11) as the surface data strengthens the usage of surface fracture analogues in the workflow (Fig. 5) and the linking of data between outcrop and the subsurface. Two other fracture sets were observed in the subsurface data. The dominant east–west set (Set 3) in the wells and the long north–south fractures (Set 4) observed in the seismic (Fig. 11). These sets are widely distributed in the main subsurface reservoirs; however, they are not observed on the surface pavements and therefore are likely to have formed between the Ordovician and Carboniferous prior to the late Permian shortening event (Gutierrez and Youn 2015).

Whilst the stylolites are observed to be widely distributed within the folded region and can act as both conduits and barriers to reservoir flow (Bruna *et al.* 2019*b*), their dynamic behaviour is unknown and therefore these features will not be considered in the modelling phase of this work.

## Dynamic modelling of the fracture network

### Hybrid fracture network modelling

Four fracture sets (Fig. 11; Table 2) were observed to be distributed throughout the system and were integrated into the hybrid model through a combination of small-scale DFN modelling (sets 1–3) and a large-scale seismic deterministic model (primarily sets 3 and 4). The DFN model was generated using the 3D fracture modelling workflow in MOVE modelling software (Petroleum Experts). This workflow involves distributing fracture sets based on field and subsurface data in a defined geocelluar volume (e.g. target reservoir volume) through several parameters (orientation, height and length ratios ($H/L$), volumetric fracture intensity ($P_{32}$) and aperture). Using the field and well data, fracture orientations were defined by azimuth, dip and Fisher distribution. Fracture lengths were determined from the pavement analysis and were combined with estimated $H/L$ ratios from the well data. Fracture intensity ($P_{32}$) was

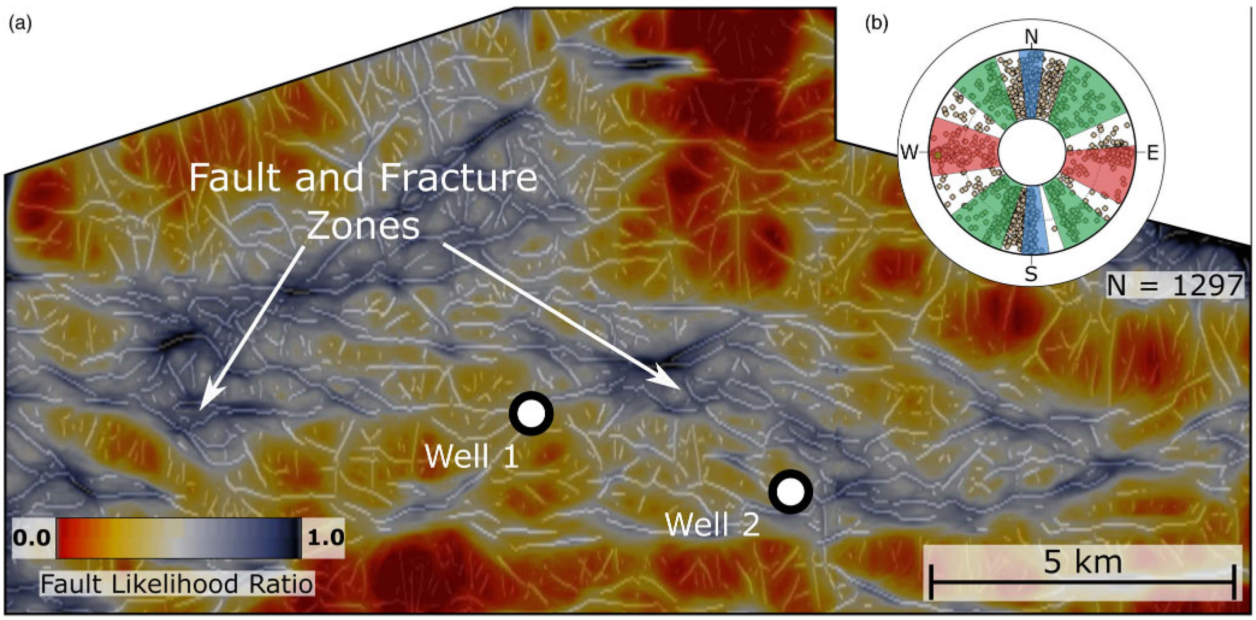


**Fig. 9.** Subsurface fracture analysis. (**a**) Fault likelihood (underlay) and thinned fault likelihood (white lineations overlay) seismic attributes showing the detected fractures in the early Paleozoic reservoirs, (**b**) Stereoplot (Schmidt projection) and strike rose diagram showing the strike orientation of the extracted fractures from the seismic analysis. Sets 1–3 are observed within seismic. An additional older set (blue: Set 4) is also interpreted and possibly related to Set 3 observed in the well data.

estimated from the pavement areal intensity as $P_{21} \approx P_{32}$ as a function of the Fisher coefficient ($K < 50$). Aperture values were defined as constant for this modelling stage and were based on previous estimates (Roskam 2016). These initial input values of the DFN modelling are shown in Table 3. The small-scale DFN modelling process generated 244 000 small fractures with total volume of $3.1 \times 10^4$ m$^3$ within the target reservoir volume ($7.3 \times 10^9$ m$^3$) and a total fracture porosity of $4.2 \times 10^{-5}$, in line with the fracture intensities measured in the outcrops and wells.

The seismic deterministic model was generated using 2D seismic slices from the TFL attribute, which created a large-scale fault and fracture network of the subsurface. The large-scale deterministic model from seismic fractures (Fig. 9) was filtered based on the boundary conditions. Fractures of less than 15 m have a higher degree of uncertainty due to the resolution of the seismic and the effects of the boundaries of the seismic data on the attribute algorithm. These lineations were not considered for analysis in the seismic model and were instead captured by the stochastic DFN model.

The identified fractures were combined with the stochastic smaller-scale DFN model to form the multiscale 2D hybrid fracture model (Fig. 12a).

To combine both models, 2D slices were generated from the 3D DFN model and overlain by the 2D seismic slices from the same depth, thus forming the 2D hybrid fracture model.

## Geometrical aperture modelling

The 2D multiscale hybrid fracture model provides the basis for further modelling of the fracture properties and dynamic flow simulations. The initial step in the dynamic simulations was modelling the fracture aperture. Fracture aperture is an important characteristic of fracture networks in the subsurface as it determines the conductivity of the network and how easily fluids can flow. It is therefore vital to understand and quantify which fractures are open (high aperture) or closed (small to zero aperture). Apertures calculated from FMI and core data can be overestimated, and therefore by using these initial

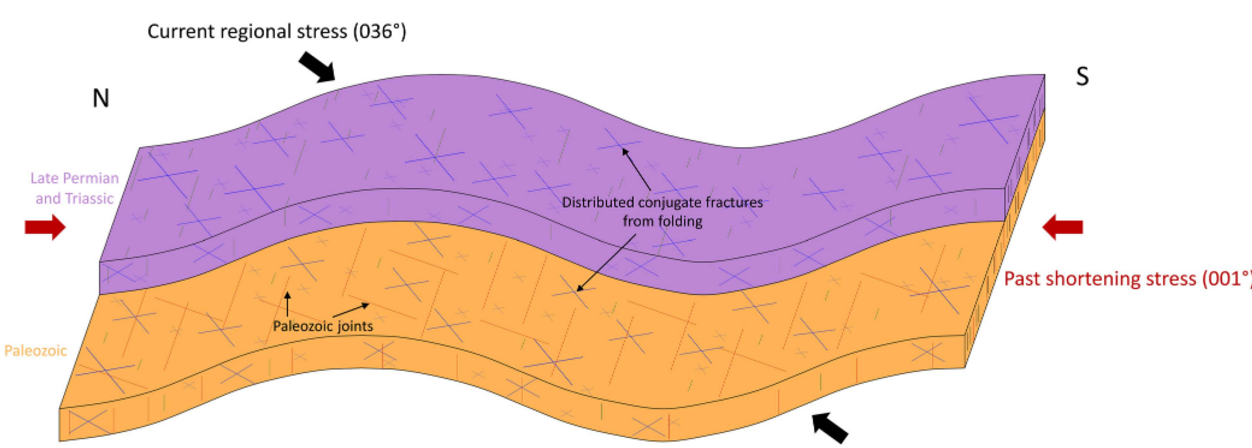


**Fig. 10.** Schematic fracture framework of the open folds showing the joint sets observed in the field (sets 1 and 2) and in the subsurface (sets 1–4). Past maximum stress orientation corresponds to the late Permian compressional phase. Current maximum stress orientation is used in aperture modelling (see Fig. 12b).

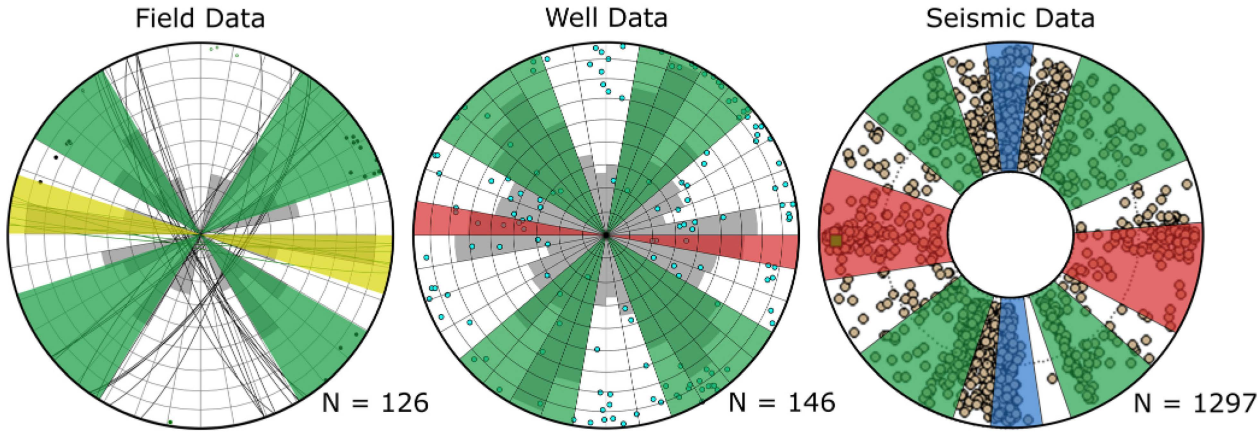


**Fig. 11.** Comparison of stereoplots (Schmidt projection) of data collected from outcrop, well and seismic. The conjugate set of fractures (green: sets 1 and 2) are observed at both small scale (outcrop and well) and large scale (seismic). Stylolites (yellow) are considered closed when observed in outcrops. Set 3 (east–west-trending fractures) is observed in wells and seismic (red). Large north–south fractures (blue: Set 4) are primarily observed in seismic.

calculations and applying fracture aperture modelling these uncertainties can be reduced (Johns *et al.* 1993).

An analytical approach was applied to the hybrid fracture model to predict the mechanical aperture of the fracture network on a 2D horizontal plane within the current stress regime (Barton and Bandis 1980; Barton 2014; Bisdom *et al.* 2016*b*).

The methodology proposed by Bisdom *et al.* (2016*b*) uses several geomechanical properties of the fractures (e.g. joint roughness coefficient (JRC) and joint compressive strength (JCS)) and the host rocks (e.g. Poisson's ratio and Young's modulus). Using GIS software, the fracture orientations and lengths can be determined. Using the fracture orientation, the angle between the fracture strike and the direction of the principal stress axis ($\sigma_1$) can be calculated, and is defined as the stress angle, $\alpha$. Through a series of analytical equations, using the stress angle, magnitude of $\sigma_1$ and the fracture properties, corrections can be made to the magnitude of the stress applied to the fractures based on fracture orientation, length and spacing. Fracture aperture ($E_n$) can be calculated using the following formula:

$$E_n = E_0 - \left(\frac{1}{v_m} + \frac{K_{ni}}{\sigma_n}\right)^{-1}$$

where $E_0$ is the constant initial aperture, $v_m$ is the maximum closure of the fracture, $K_{ni}$ is the initial stiffness of the rock and $\sigma_n$ is the compressive stress for each fracture calculated previously. $E_0$, $v_m$ and $K_{ni}$ are functions of several geomechanical properties of the host rock (JCS, JRC and uniaxial compressive strength (UCS, $\sigma_c$)) (Barton and Bandis 1980; Barton 2014).

Geomechanical properties of the rock (JCS, JRC, UCS, Poisson's ratio and Young's modulus) used in this modelling process have been derived from well data ($V_P$ and $V_S$) and *in situ* and laboratory testing (e.g. multistage triaxial compression testing) (confidential source). The maximum horizontal stress orientation was estimated to be N036° and the magnitude (maximum and minimum horizontal stress) was obtained from well breakouts (Grech and Addala 2014).

**Table 2.** Fracture sets observed in outcrop, well and seismic

| Set | 1 | 2 | 3 | 4 |
|---|---|---|---|---|
| Strike (°) | 150 | 212 | 269 | 001 |
| Dip angle (°) | 80 | 85 | 87 | 87 |
| Data source | Outcrop, well, seismic | Outcrop, well, seismic | Well, seismic | Seismic |

## Aperture modelling results

The results of the aperture modelling (Fig. 12b) show that the apertures that are perpendicular (Set 1: 150°) to the main horizontal stress (036°) experience the highest stress and lowest aperture (0.170 mm), whilst the fractures parallel to this main stress (Set 2: 212°) experience lower stresses and higher apertures (0.220 mm).The east–west-trending joints show variations in stress applied and aperture, depending on the size of fracture. The average aperture across all sets was 0.194 mm. Several studies have previously shown that there are scaling relationships with fracture aperture and stress; however, these can be variable within carbonate lithologies and outcrops (Hooker *et al.* 2012, 2014; Bisdom *et al.* 2016*a*, *b*). Shear displacement results are heavily influenced by fracture length, and therefore the longer fractures show the most displacement (Baghbanan and Jing 2008 and references therein). These fractures could provide enhanced flow paths for fluids. The conjugate fracture orientated at 212° shows a higher aperture than the conjugate set orientated at 150°. Therefore, in general, the sets of fracture conjugates contain unequal aperture size, one set wider than the other, and could have an impact on connectivity. Connectivity analysis of the hybrid fracture model shows that 75% of the fractures are connected by either crossing or abutment intersections, whilst 25% of fractures are isolated, which is in within the rage of connections per line for a good system percolation (Balberg *et al.* 1984; Manzocchi 2002; Sanderson and Nixon 2015). Combined with the aperture results, this analysis shows that whilst the fracture network is well connected, certain fracture sets will hinder flow. However, good connectivity overall in the network should enable better flow from the small open fractures through to the large fractures.

## Permeability upscaling through fluid-flow simulations

To further illustrate the influence of the fracture network on fluid flow within the reservoir, we upscaled the model using the finite-

**Table 3.** Input values for the DFN model

| Set | 1 | 2 | 3 |
|---|---|---|---|
| Strike (°) | 150 | 212 | 269 |
| Dip angle (°) | 80 | 85 | 87 |
| Intensity ($P_{32}$) ($m^2\ m^{-3}$) | 0.063 | 0.063 | 0.036 |
| Length exponent | 1.8 | 1.8 | 1.8 |
| Initial aperture (mm) | 0.94 | 0.94 | 0.94 |
| Notes | Conjugate 1 | Conjugate 2 | Subsurface fracture |

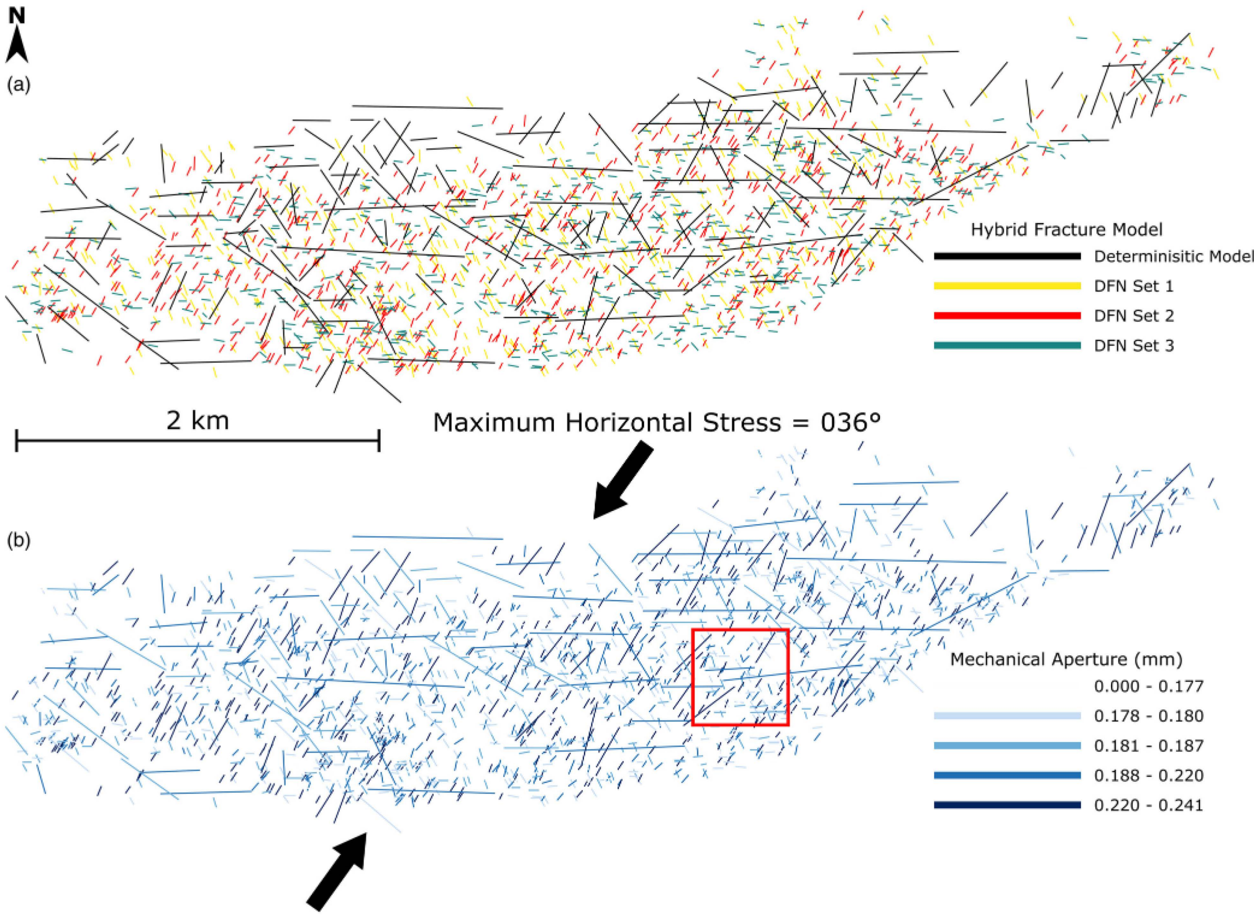


**Fig. 12.** (**a**) Multiscale 2D hybrid fracture model generated from the DFN model (field and well data) and the deterministic model (seismic data). (**b**) Analytical mechanical aperture model showing the variations in fracture aperture caused by the present-day stress (036°) regime in the Southern Chotts–Jeffara Basin. The red box indicates the area used for numerical simulation.

element method to determine permeability and obtain a 2D permeability tensor. For our simulations we used the open-source simulator REDBACK (Poulet *et al.* 2017) based on the MOOSE Framework (Permann *et al.* 2020) that treats fractures as infinitely thin geometrical features (lower-dimensional elements) to reduce complexities and increase efficiency within the simulation, which is an advantage over other methods used to obtain the tensor (Cacace and Jacquey 2017; Poulet *et al.* 2021).

A sample fracture network (Fig. 13a) from the 2D hybrid model (Fig. 12) was meshed using Gmsh (Geuzaine and Remacle 2009), which is a 3D finite-element grid generator that allows independence between fractures and the matrix. Fracture sets are defined as physical groups, which enables them to be used within the simulations as lower-dimensional elements. Using empirical cubic laws based on the Hagen–Poiseuille solution of the Navier–Stokes equation, permeability along individual fractures (longitudinal permeability) was approximated (Table 4) from the analytically modelled apertures (Snow 1969; Witherspoon *et al.* 1980). These are within the range of permeability values measured from other aperture and fault permeability simulations (Cappa and Rutqvist 2011). It is unknown whether these fractures are conduit-barrier systems and therefore the transverse permeability across the fracture is kept constant (0.01 mD), thus treating the fractures mainly as barriers to transversal flow. To obtain the upscaled 2D permeability tensor of the pavement model (Fig. 13b), the simulation was run twice along each perpendicular horizontal pressure gradient (Fig. 13c, d).

The upscaled permeability tensor (Table 5) and ellipse of the fracture network (Fig. 13b) further highlights how the fluid flow within the network is heavily influenced by the fracture set orientated at 212° and the larger fractures within that orientation. These results also express how the small-scale networks complement the large-scale network to provide good flow pathways, improving connectivity and percolation within the reservoir.

## Discussion

### Fractures in the Southern Chotts–Jeffara Basin

The late Permian–early Triassic folding created a distributed fracture network in the Triassic and Paleozoic units. Fractures on the surface are generally organized as conjugate systems populating open fold structures. To allow for a distributed network across the folds, fracturing during shortening occurred early on during the LPS phase (e.g. Bergbauer and Pollard 2004). However, previous interpretations of the fractures around the Tebaga of Medenine have attributed fracturing in the Permian units to damage zones along faults (Raulin *et al.* 2011). The extensive outcrop and subsurface data analysis (Figs 6–9; also see the Supplementary material) presented in this study demonstrates that these fractures are likely to be distributed throughout the whole region. Furthermore, carbonate rocks were susceptible to early fracturing during the LPS stage due to the brittle behaviour of the rock mechanics, which corresponds to the rock types observed in outcrop such as the Permian units (e.g. Swanson 1988; Tavani *et al.* 2011; Branellec *et al.* 2015). Variations in fracture orientations and intensity were observed in outcrop, and were primarily concentrated around localized fault

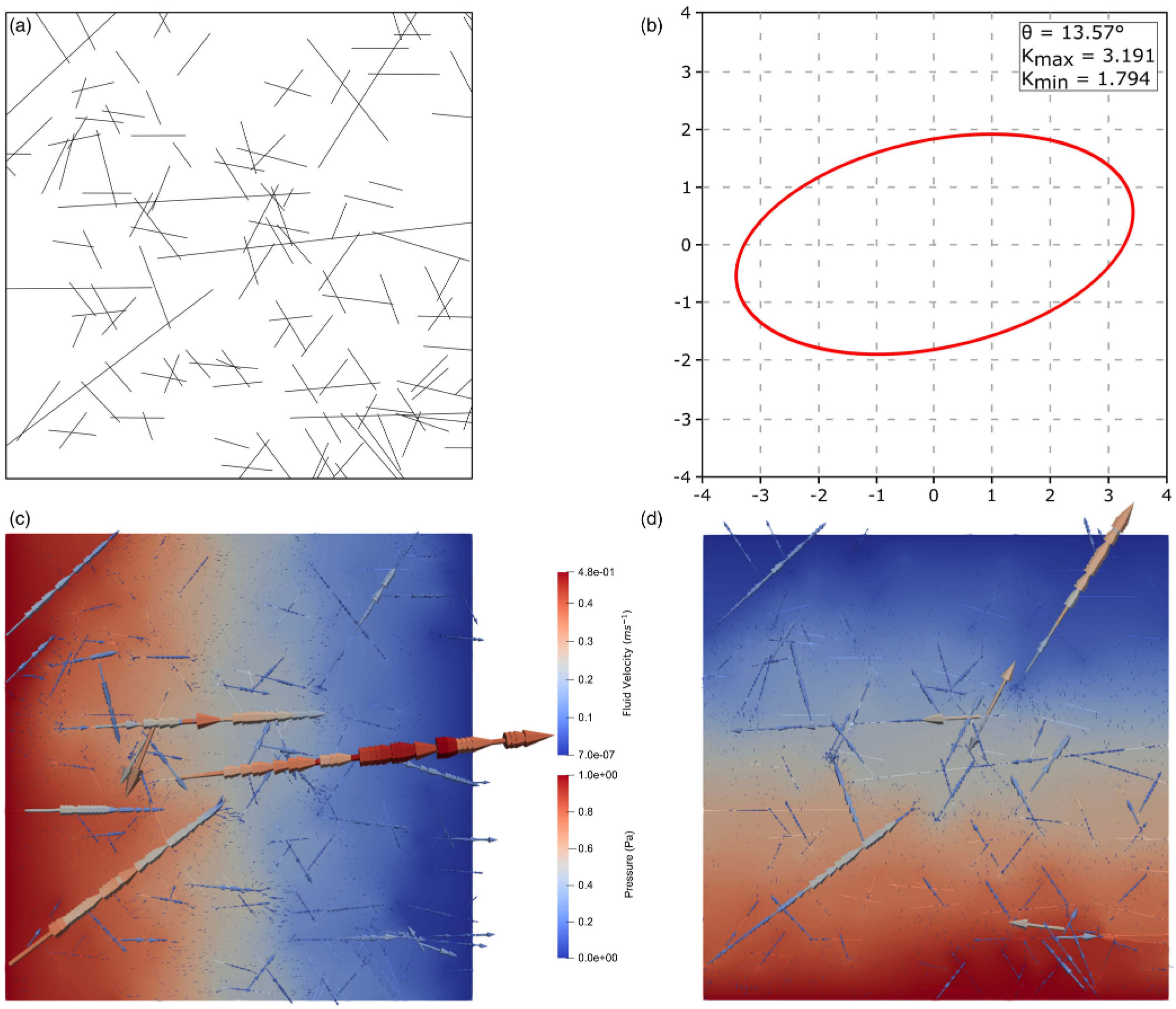


**Fig. 13** (**a**) Sample fracture network from the hybrid fracture model (Fig. 12b). (**b**) Calculated 2D permeability tensor showing similar orientations to the large-scale fractures and Set 2. (**c**) Pressure distributions and fluid-flow velocity vectors for flow in the $Y$ direction. (**d**) Pressure distributions and fluid-flow velocity for flow in the $X$ direction. $\theta$, principal axis direction of fluid flow; $K_{\max}$, maximum value of permeability found on the principal axis; $K_{\min}$, minimum value of permeability found on the principal axis.

zones and, in particular, in the Kirchaou area (pavements 2 and 3). This area within the Southern Chotts–Jeffara Basin has been influenced by the Jeffara Fault System, formed on the basin margin of the Neo-Tethys Ocean between the Jurassic and Cretaceous (e.g. Bouaziz 1995; Mejri *et al.* 2006; Gabtni *et al.* 2009; Frizon de Lamotte *et al.* 2011; Raulin *et al.* 2011; Bahrouni *et al.* 2014; El Rabia *et al.* 2018; Soumaya *et al.* 2020).

## Applicability of hybrid fracture modelling and simulation

The multiscale integrated fracture model allows for the representation of fractures observed at both large-scale (seismic) and small-scale (outcrop and well) in a subsurface model of the Southern Chotts-Jeffara basin. The three modelled sets of fracture (Table 3) in the DFN model represented the small-scale fractures observed in the outcrop and well data. Other small-scale structural features, such as stylolites, were observed in the field. These features were observed to be primarily closed (cemented) and although stylolites can reach great lengths (Laronne Ben-Itzhak *et al.* 2014), these are commonly associated with sedimentary processes resulting in bedding-parallel stylolites. Instead, the stylolites observed in the Tebaga of Medenine are near vertical (Figs 6 & 7a, b, d) and therefore related to tectonic processes. As the dynamic behaviour of these features is unknown as depth, they were not considered in the modelling workflow (Ebner *et al.* 2009; Piazolo *et al.* 2019).

The DFN modelling approach enabled small-scale fractures, which would not be captured at the scale of the reservoir, to be captured in a model. These fracture sets play important roles in

**Table 4.** Parameters for the 2D numerical permeability upscaling

| Set | 1 | 2 | 3 | 4 |
|---|---|---|---|---|
| Aperture (mm) | 0.215 | 0.223 | 0.185 | 0.177 |
| Longitudinal permeability (mD) | 0.828 | 0.919 | 0.527 | 0.464 |

**Table 5.** The 2D permeability tensor of the fracture network

| | |
|---|---|
| [2.9571 | 0.2383] |
| [0.1963 | 2.0278] |

connectivity and percolation through the network, as shown by the high concentration of cross-cutting and abutting fracture intersections in the connectivity analysis of the model. Given the stochastic nature of DFN modelling, uncertainties will arise during the process (Jing and Stephansson 2007; Elfeel and Geiger 2012; Karatalov *et al.* 2017). By using multiple data sources, we can better drive the DFN approach to improve its validity, whilst also using the fracture drivers to link our surface and subsurface sources in the region together.

Whilst our DFN model captures a realization of the small fractures in the subsurface, it remains only a single realization. Conducting a full statistical uncertainty distribution and ensemble analysis of the fracture network models was outside the scope of this research. The single realization offers a first hint on fracture behaviour at depth and would need to be studied further in the future (Elmouttie *et al.* 2014). Other equiprobable realizations compatible with our data would generate slightly different geometries and connectivity, and possibly fit the dynamic model better than the model presented in this research. Therefore, this limitation concerning the modelling results and interpretation should be noted.

Combining a deterministic model with the DFN model allows a reduction in the uncertainties associated with the stochastic approach. This additional fracture model allows fractures observed directly in the subsurface to be integrated whilst also representing fractures at larger scales. There are certain approaches that also aim to integrate deterministic and stochastic methods; however, the integration of seismic, well and outcrop data with fracture drivers is limited (e.g. Belayneh *et al.* 2009; Pan *et al.* 2019). Many of these existing approaches focus on small-scale fractures and networks, and expanding these processes to large-scale networks and regions can be computationally and time expensive (e.g. Jung *et al.* 2013; Berrone *et al.* 2019; Boersma *et al.* 2021; Ern *et al.* 2022). Integrating the deterministic fracture models from seismic data with the stochastic DFN model builds on the concept of using training images within the modelling process and capturing the multiscale dimensions of networks (e.g. Chugunova *et al.* 2017; Bruna *et al.* 2019*c*). The workflow used in this study is an effective method of integrating fractures across scales and data sources, and efficiently modelling fracture and fluid-flow properties to assess the influence of networks within a large subsurface region.

The analytical aperture modelling applied to the 2D fracture network aids a better understanding of how the fracture network is behaving at depth under *in situ* and regional stresses. Subsurface stress anisotropy determined from well evidence provides data from

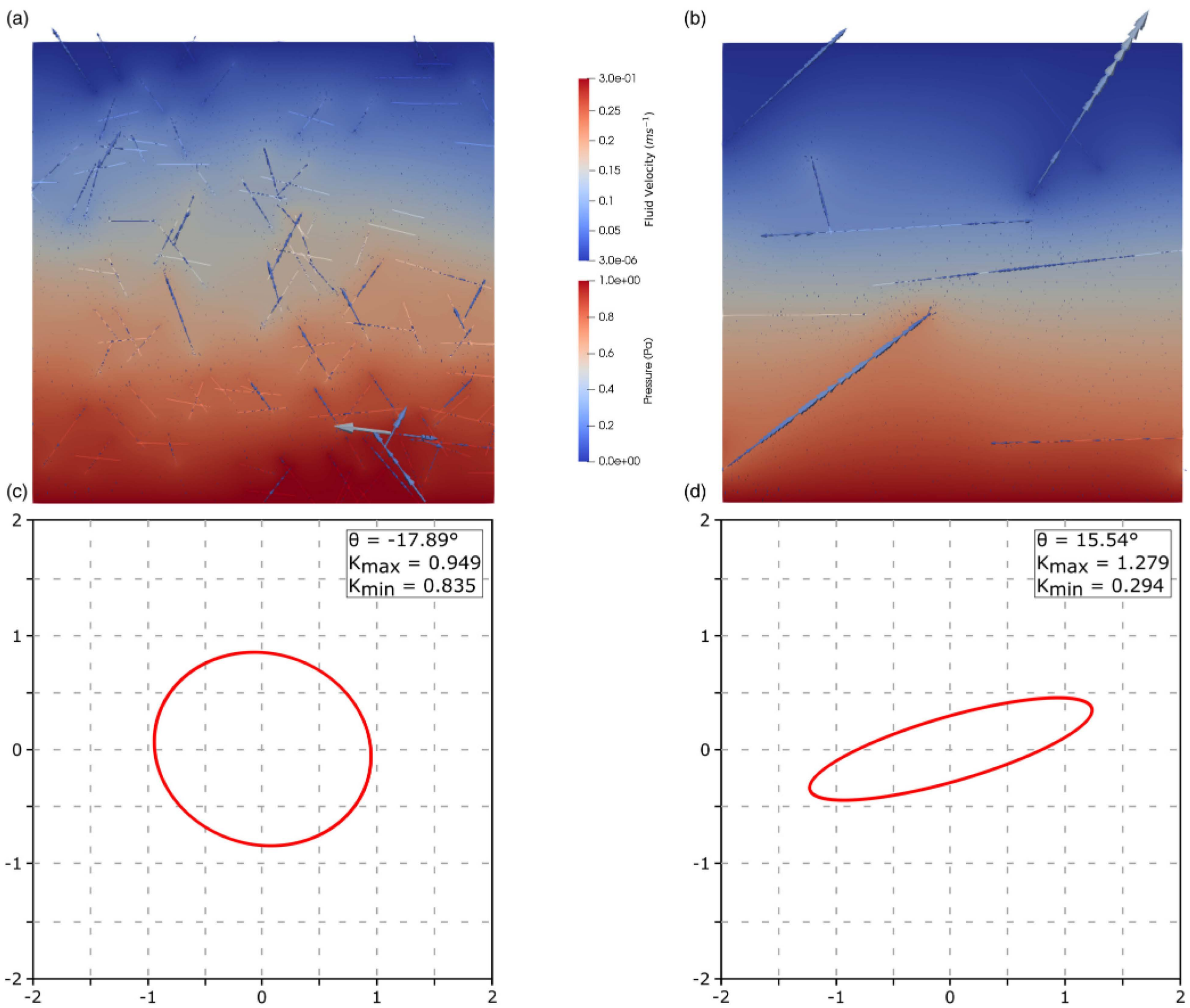


**Fig. 14** Comparison of pressure distribution and fluid-flow velocity vectors for flow in the *Y* direction between (**a**) the small-scale network and (**b**) the large-scale network. 2D permeability tensors of (**c**) the small-scale network and (**d**) the large-scale network show variations and a reduction in permeability from a combined network (Fig. 13). $\theta$, principal axis direction of fluid flow; $K_{max}$, maximum value of permeability found on the principal axis; $K_{min}$, minimum value of permeability found on the principal axis.

which the aperture modelling can be applied (RPS Energy 2018; Serinus Energy 2022). This method relates several geometrical fracture parameters to stresses and displacements controlled by fracture length, block size and spacing that define aperture sizing, and therefore negates the requirement to run computationally expensive numerical methods to calculate the aperture (Olson 2003; Olson and Schultz 2011; Bisdom *et al.* 2016*b*). Furthermore, we applied a numerical approach to fluid-flow simulations and permeability upscaling (Smith *et al.* 2022). This method allows fracture properties to be integrated numerically using lower-dimensional elements rather than discretely within the mesh, which creates more efficient simulations that are computationally inexpensive (Cacace and Jacquey 2017; Poulet *et al.* 2021; Smith *et al.* 2022). This method also accounts for variations in fracture aperture by set (orientation and length), which can significantly impact the fluid-flow orientation and velocity at higher scales (Smith *et al.* 2022).

### Implications of the fracture network on fluid flow

The results of the aperture modelling and simulation show the effects of the both the small-scale and large-scale fractures on fluid flow. The large-scale fracture network clearly shows an impact on permeability within the reservoir (Fig. 13b), and the output from the simulations (Fig. 13c, d) indicate that the large-scale fractures are acting as conduits to flow. However, the small-scale fractures (in particular, fractures orientated at 212°) are also a vital component that influences flow behaviour in the system. The small-scale fracture network improves the connectivity between the large-scale fractures, increasing permeability by three times when compared with a network formed of only the larger network (Fig. 14). The fractures at each scale complement each other, enabling improved flow through the multiscale fracture network at depth.

In low-permeability reservoirs such as the Permian units, these fracture networks are likely have a large impact on the fluid-flow orientation and velocity, and will be important for reservoir management and planning. However, in other reservoirs, such as the highly permeable Paleozoic and TAGI sandstones, the fractures could complement matrix permeability as conduits to flow or, negatively, cause compartmentalization around fracture flow zones (Besser and Hamed 2019; Baouche *et al.* 2022; Bruna *et al.* 2022*a*).

Pressure transient analysis from previous well testing of the field has identified dual-porosity behaviour within the reservoir (RPS Energy 2018; Serinus Energy 2022). While current models of the field have not integrated fracture networks, it has been observed that evidence of highly fractured areas has corresponded to increased production rates, and that the vertical permeability is enhanced by fracture flow and improved performance of wells. However, variations in fracture network properties observed from well to well indicate that whilst fractures increase flow in some areas, it could also obstruct flow. Therefore, understanding the influence of the fracture networks is vital for enhancing and managing the reservoirs in the Southern Chotts–Jeffara Basin.

## Conclusions

A distributed fracture network across the Southern Chotts–Jeffara Basin was formed during a late Permian–early Triassic regional compressional event that resulted in the onset of large open folds across the basin. Through observation and interpretation of surface and subsurface data using unconventional and modern methods, we integrated fractures at various scales into a hybrid fracture model from which analytical and numerical calculations on network properties were undertaken. Through surface fracture characterization, two main fracture orientations (sets 1 and 2) were observed conjugated and distributed across the basin; these were formed during the layer-parallel shortening phase of regional folding. Pavement analysis of the fractures quantified the orientations, areal intensity, length and connectivity of these small-scale fractures. The open folds provide a link between fracture generations on the surface and at depth. Subsurface fracture characterization of the western region of the basin found the same conjugate fracture sets (sets 1 and 2), in addition to several other widely distributed fracture sets (sets 3 and 4) within the Paleozoic units.

Stochastic DFN modelling of the small-scale fractures (up to 10 m) was driven primarily by well data and was complemented by data from surface pavements to make reliable predictions of the subsurface fracture architecture. Seismic attribute analysis allowed the tracing of large-scale fractures (up to 200 m) directly in the subsurface to create a deterministic model. By combining both models, a multiscale hybrid fracture model of the reservoirs was generated. Analytical aperture modelling based on current *in situ* and regional stresses provided additional fracture parameters for numerical analysis of the subsurface fluid flow. Permeability upscaling showed the influence of large-scale fractures on flow orientation and velocity, and was complimented by small-scale fractures orientated at 212° (Set 2), which provide conduit links between the larger features. This shows that fractures influence fluid-flow behaviour in the subsurface and could improve reservoir permeability within the basin.

**Acknowledgements** Mazarine Energy B.V. is thanked for allowing us access to and the use of well and seismic data. Petroleum Experts and dGB Earth Sciences are thanked for software licence access to MOVE and OpendTect, respectively. Salma Ben Amor (Baker Hughes) is thanked for sharing expertise and knowledge on the Southern Chotts–Jeffara Basin and the reservoirs in the region. Geologists at Mazarine Energy Tunisia, Entreprise Tunisienne d'Activités Pétrolières (ETAP), National Office of Mines (ONM) and from the University of Tunis El Manar are thanked for their insights and constructive discussions at field outcrops in Tunisia. Ibrahim Attia and an anonymous reviewer are warmly thanked for their constructive remarks.

**Author contributions** **RYS**: conceptualization (supporting), data curation (equal), formal analysis (lead), investigation (equal), methodology (equal), project administration (supporting), validation (equal), visualization (lead), writing – original draft (lead); **P-OB**: conceptualization (equal), data curation (equal), investigation (equal), methodology (equal), software (equal), supervision (lead), validation (lead), visualization (equal), writing – review & editing (supporting); **AN**: data curation (supporting), investigation (supporting), resources (equal); **GB**: conceptualization (lead), data curation (supporting), funding acquisition (lead), methodology (equal), project administration (lead), supervision (equal), validation (equal), writing – review & editing (equal).

**Funding** This work was funded by the North African Research Group (NARG), Mazarine Energy and Technische Universiteit Delft.

**Competing interests** The authors declare that they have no known competing financial interests or personal relationships that could have appeared to influence the work reported in this paper.

**Data availability** We have provided some datasets generated during and/or analysed during the current study. Some datasets are not publicly available due to confidentiality requests from funding company but can be requested from the corresponding author.

## References

Baghbanan, A. and Jing, L. 2008. Stress effects on permeability in a fractured rock mass with correlated fracture length and aperture. *International Journal of Rock Mechanics and Mining Sciences*, **45**, 1320–1334, https://doi.org/10.1016/j.ijrmms.2008.01.015

Bahrouni, N., Bouaziz, S. *et al.* 2014. Neotectonic and seismotectonic investigation of seismically active regions in Tunisia: a multidisciplinary approach. *Journal of Seismology*, **18**, 235–256, https://doi.org/10.1007/s10950-013-9395-y

Balberg, I., Anderson, C.H., Alexander, S. and Wagner, N. 1984. Excluded volume and its relation to the onset of percolation. *Physical Review B*, **30**, 3933, https://doi.org/10.1103/PhysRevB.30.3933

Balti, T., Nasr, I.H. and Inoubli, M.H. 2018. Petrophysical characterization of upper Permian reservoir in southern Tunisia. *In*: Sundararajan, N., Eshagh, M., Saibi, H., Meghraoui, M., Al-Garni, M. and Giroux, B. (eds) *On Significant Applications of Geophysical Methods. CAJG 2018*. Advances in Science, Technology & Innovation. Springer, Cham, Switzerland, 169–171, https://doi.org/10.1007/978-3-030-01656-2_38

Baouche, R., Sen, S. and Feriel, H.A. 2022. Determining shear failure gradient and optimum drilling mud window in the Ourhoud oil field, Berkine Basin, Algeria. *Interpretation*, **10**, SF1–SF7, https://doi.org/10.1190/INT-2021-0134.1

Barton, N. 2014. Non-linear behaviour for naturally fractured carbonates and frac-stimulated gas-shales. *First Break*, **32**, https://doi.org/10.3997/1365-2397.2014011

Barton, N. and Bandis, S. 1980. Technical note: some effects of scale on the shear strength of joints. *International Journal of Rock Mechanics and Mining Sciences*, **17**, 69–73, https://doi.org/10.1016/0148-9062(80)90009-1

Belayneh, M.W., Matthai, S.K., Blunt, M.J. and Rogers, S.F. 2009. Comparison of deterministic with stochastic fracture models in water-flooding numerical simulations. *AAPG Bulletin*, **93**, 1633–1648, https://doi.org/10.1306/07220909031

Belfield, W.C. and Sovich, J.P. 1995. Fracture statistics from horizontal wellbores. *Journal of Canadian Petroleum Technology*, **34**, https://doi.org/10.2118/95-06-04

Ben Ferjani, A., Burollet, P. and Mejri, F. 1990. *Petroleum Geology of Tunisia*, Entreprise Tunisienne d'Activités Pétrolières (E.T.A.P.), Tunis.

Bergbauer, S. and Pollard, D.D. 2004. A new conceptual fold-fracture model including prefolding joints, based on the Emigrant Gap anticline, Wyoming. *Geological Society of America Bulletin*, **116**, 294–307, https://doi.org/10.1130/B25225.1

Berrone, S., Scialo, S. and Vicini, F. 2019. Parallel meshing, discretization, and computation of flow in massive discrete fracture networks. *SIAM Journal on Scientific Computing*, **41**, C317–C338, https://doi.org/10.1137/18M1228736

Besser, H. and Hamed, Y. 2019. Causes and risk evaluation of oil and brine contamination in the Lower Cretaceous Continental Intercalaire aquifer in the Kebili region of southern Tunisia using chemical fingerprinting techniques. *Environmental Pollution*, **253**, 412–423, https://doi.org/10.1016/j.envpol.2019.07.020

Bisdom, K., Gauthier, B.D.M., Bertotti, G. and Hardebol, N.J. 2014. Calibrating discrete fracture-network models with a carbonate three-dimensional outcrop fracture network: Implications for naturally fractured reservoir modeling. *AAPG Bulletin*, **98**, 1351–1376, https://doi.org/10.1306/02031413060

Bisdom, K., Bertotti, G. and Nick, H.M. 2016*a*. The impact of different aperture distribution models and critical stress criteria on equivalent permeability in fractured rocks. *Journal of Geophysical Research: Solid Earth*, **121**, 4045–4063, https://doi.org/10.1002/2015JB012657

Bisdom, K., Bertotti, G. and Nick, H.M. 2016*b*. A geometrically based method for predicting stress-induced fracture aperture and flow in discrete fracture networks. *AAPG Bulletin*, **100**, 1075–1097, https://doi.org/10.1306/02111615127

Bodin, S., Petitpierre, L., Wood, J., Elkanouni, I. and Redfern, J. 2010. Timing of Early to Mid-Cretaceous tectonic phases along North Africa: new insights from the Jeffara escarpment (Libya–Tunisia). *Journal of African Earth Sciences*, **58**, 489–506, https://doi.org/10.1016/j.jafrearsci.2010.04.010

Boersma, Q., Hardebol, N., Barnhoorn, A. and Bertotti, G. 2018. Mechanical factors controlling the development of orthogonal and nested fracture network geometries. *Rock Mechanics and Rock Engineering*, **51**, 3455–3469, https://doi.org/10.1007/s00603-018-1552-8

Boersma, Q.D., Bruna, P.O., de Hoop, S., Vinci, F., Tehrani, A.M. and Bertotti, G. 2021. The impact of natural fractures on heat extraction from tight Triassic sandstones in the West Netherlands Basin: a case study combining well, seismic and numerical data. *Netherlands Journal of Geoscience*, **100**, E6, https://doi.org/10.1017/njg.2020.21

Bonnet, E., Bour, O., Odling, N.E., Davy, P., Main, I., Cowie, P. and Berkowitz, B. 2001. Scaling of fracture systems in geological media. *Reviews of Geophysics*, **39**, 347–383, https://doi.org/10.1029/1999RG000074

Bouaziz, S. 1995. *Etude de la tectonique cassante dans la plate-forme et l'Atlas Sahariens (Tunisie méridionale): Evolution des paléochamps de contraintes et implications géodynamiques*. PhD thesis, l'Université de Tunis II, Tunis, Tunisia.

Bouaziz, S. and Ben Salem, H. 1987. *Carte géologique au 1/100 000 de Kirchaou. Feuille No. 100*. National Office of Mines (ONM), Tunis.

Bouaziz, S. and M'Hadhbi, M. 1987. *Carte géologique au 1/100 000 de Sidi Toui. Feuille No. 109*. National Office of Mines (ONM), Tunis.

Bouaziz, S., Barrier, E., Soussi, M., Turki, M.M. and Zouari, H. 2002. Tectonic evolution of the northern African margin in Tunisia from paleostress data and sedimentary record. *Tectonophysics*, **357**, 227–253, https://doi.org/10.1016/S0040-1951(02)00370-0

Bourbiaux, B. 2010. Fractured reservoir simulation: a challenging and rewarding issue. *Oil & Gas Science and Technology – Revue de l'Institut Français du Pétrole*, **65**, 227–238, https://doi.org/10.2516/ogst/2009063

Branellec, M., Callot, J.P., Nivière, B. and Ringenbach, J.C. 2015. The fracture network, a proxy for mesoscale deformation: constraints on layer parallel shortening history from the Malargüe fold and thrust belt, Argentina. *Tectonics*, **34**, 623–647, https://doi.org/10.1002/2014TC003738

Brouwer, F. and Huck, A. 2011. An integrated workflow to optimize discontinuity attributes for the imaging of faults. *In*: Marfurt, K.J., Gao, D. *et al.* (eds) *Attributes: New Views on Seismic Imaging – Their Use in Exploration and Production: Proceedings of the 31st Annual GCSSEPM Foundation Bob F. Perkins Research Conference*. Gulf Coast Section SEPM (GCSSEPM), Houston, TX, 496–533, https://doi.org/10.5724/gcs.11.31.0496

Brown, A.B. 2001. Understanding seismic attributes. *Geophysics*, **66**, 47–48, https://doi.org/10.1190/1.1444919

Bruna, P.-O., Bertotti, G., Ben Amor, S., Nasri, A. and Ouahchi, S. 2019*a*. Analysis of the pre- and post variscan unconformity deformations: new insights for the characterisation of the Ordovician and Triassic reservoirs in the Southern Chotts Basin, Tunisia. Paper presented at the PESGB Africa E&P Conference 2019, 1–2 October 2019, London, UK.

Bruna, P.-O., Lavenu, A.P., Matonti, C. and Bertotti, G. 2019*b*. Are stylolites fluid-flow efficient features? *Journal of Structural Geology*, **125**, 270–277, https://doi.org/10.1016/j.jsg.2018.05.018

Bruna, P.-O., Straubhaar, J., Prabhakaran, R., Bertotti, G., Bisdom, K., Mariethoz, G. and Meda, M. 2019*c*. A new methodology to train fracture network simulation using multiple point statistics. *Solid Earth*, **10**, 537–559, https://doi.org/10.5194/se-10-537-2019

Bruna, P.-O., Smith, R.Y., Ben Amor, S., Masi, B., Moscariello, A. and Bertotti, G. 2020. Permian to Jurassic shortening controlling thickness changes and fracture patterns in the Chotts and Jeffara Basins, Central Tunisia: implications for petroleum reservoirs. Paper presented at the 3rd Conference of the Arabian Journal of Geosciences, 2–5 November 2020, online.

Bruna, P.-O., Bertotti, G., Amor, S.B., Nasri, A. and Ouahchi, S. 2022*a*. Vertical movements and petroleum system modelling in the southern Chotts Basin, Central Tunisia. *In*: Meghraoui, M., Sundararajan, N. *et al.* (eds) *Advances in Geophysics, Tectonics and Petroleum Geosciences: Proceedings of the 2nd Springer Conference of the Arabian Journal of Geosciences (CAJG-2), Tunisia 2019*. Springer Nature, 619–622, https://doi.org/10.1007/978-3-030-73026-0_137

Bruna, P.-O., Dixon, R., Bertotti, G., Lovell-Kennedy, J. and Redfern, J. 2022*b*. A new Permo-Triassic model for Northern Africa: challenging the prevailing models. Paper presented at the AAPG/EAGE MEDINA Conference and Exhibition, 12–14 September 2022, Tunis, Tunisia.

Burollet, P.F. 1991. Structures and tectonics of Tunisia. *Tectonophysics*, **195**, 359–369, https://doi.org/10.1016/0040-1951(91)90221-D

Cacace, M. and Jacquey, A.B. 2017. Flexible parallel implicit modelling of coupled thermal–hydraulic–mechanical processes in fractured rocks. *Solid Earth*, **8**, 921–941, https://doi.org/10.5194/se-8-921-2017

Cacas, M.C., Daniel, J.M. and Letouzey, J. 2001. Nested geological modelling of naturally fractured reservoirs. *Petroleum Geoscience*, **7**, S43–S52, https://doi.org/10.1144/petgeo.7.S.S43

Cappa, F. and Rutqvist, J. 2011. Modeling of coupled deformation and permeability evolution during fault reactivation induced by deep underground injection of $CO_2$. *International Journal of Greenhouse Gas Control*, **5**, 336–346, https://doi.org/10.1016/j.ijggc.2010.08.005

Chilès, J.P. 2005. Stochastic modeling of natural fractured media: a review. *In*: Leuangthong, O. and Deutsch, C.V. (eds) *Geostatistics Banff 2004*. Quantitative Geology and Geostatistics, **14**. Springer, Dordrecht, The Netherlands, 285–294, https://doi.org/10.1007/978-1-4020-3610-1_29

Chopra S. and Marfurt K.J. 2007. *Seismic Attributes for Prospect Identification and Reservoir Characterization*. Society of Exploration Geophysicists, Tulsa, OK.

Chugunova, T., Corpel, V. and Gomez, J.P. 2017. Explicit fracture network modelling: from multiple point statistics to dynamic simulation. *Mathematical Geosciences*, **49**, 541–553, https://doi.org/10.1007/s11004-017-9687-9

Cruz, F., Roehl, D. and do Amaral Vargas, E., Jr 2019. An XFEM implementation in Abaqus to model intersections between fractures in porous rocks. *Computers and Geotechnics*, **112**, 135–146, https://doi.org/10.1016/j.compgeo.2019.04.014

Darcel, C., Bour, O., Davy, P. and De Dreuzy, J.R. 2003. Connectivity properties of two-dimensional fracture networks with stochastic fractal correlation. *Water Resources Research*, **39**, 1272, https://doi.org/10.1029/2002WR001628

Dershowitz, W.S. and Herda, H.H. 1992. Interpretation of fracture spacing and intensity. *In: 33rd US Symposium on Rock Mechanics, Santa Fe, NM, June 1992*. American Rock Mechanics Association (ARMA), Alexandria, VA, 757–766.

Dhaoui, M., Gabtni, H., Jallouli, C., Jleilia, A., Mickus, K.L. and Turki, M.M. 2014. Gravity analysis of the Precambrian basement topography associated with the northern boundary of Ghadames basin (southern Tunisia). *Journal of Applied Geophysics*, **111**, 299–311, https://doi.org/10.1016/j.jappgeo.2014.10.014

Ebner, M., Koehn, D., Toussaint, R. and Renard, F. 2009. The influence of rock heterogeneity on the scaling properties of simulated and natural stylolites. *Journal of Structural Geology*, **31**, 72–82, https://doi.org/10.1016/j.jsg.2008.10.004

Elfeel, M.A. and Geiger, S. 2012. Static and dynamic assessment of DFN permeability upscaling. Paper SPE-154369-MS presented at the SPE Europec/EAGE Annual Conference, 4–7 June 2012, Copenhagen, Denmark, https://doi.org/10.2118/154369-MS

Elmouttie, M.K., Krähenbühl, G., Poropat, G.V. and Kelso, I. 2014. Stochastic representation of sedimentary geology. *Rock Mechanics and Rock Engineering*, **47**, 507–518, https://doi.org/10.1007/s00603-013-0411-x

El Rabia, A., Inoubli, M.H., Ouaja, M., Abidi, O., Sebei, K. and Jlailia, A. 2018. Salt tectonics and its effect on the structural and sedimentary evolution of the Jeffara Basin, Southern Tunisia. *Tectonophysics*, **744**, 350–372, https://doi.org/10.1016/j.tecto.2018.07.015

Ern, A., Hédin, F., Pichot, G. and Pignet, N. 2022. Hybrid high-order methods for flow simulations in extremely large discrete fracture networks. *SMAI Journal of Computational Mathematics*, **8**, 375–398, https://doi.org/10.5802/smai-jcm.92

Fekirine, B. and Abdallah, H. 1998. Palaeozoic lithofacies correlatives and sequence stratigraphy of the Saharan platform, Algeria. *Geological Society, London, Special Publications*, **132**, 97–108, https://doi.org/10.1144/GSL.SP.1998.132.01.05

Frizon de Lamotte, D., Raulin, C., Mouchot, N., Wrobel-Daveau, J.C., Blanpied, C. and Ringenbach, J.C. 2011. The southernmost margin of the Tethys realm during the Mesozoic and Cenozoic: Initial geometry and timing of the inversion processes. *Tectonics*, **30**, TC3002, https://doi.org/10.1029/2010TC002691

Frizon de Lamotte, D., Tavakoli-Shirazi, S. *et al.* 2013. Evidence for late Devonian vertical movements and extensional deformation in northern Africa and Arabia: integration in the geodynamics of the Devonian world. *Tectonics*, **32**, 107–122, https://doi.org/10.1002/tect.20007

Gabtni, H., Jallouli, C., Mickus, K.L., Zouari, H. and Turki, M.M. 2009. Deep structure and crustal configuration of the Jeffara basin (Southern Tunisia) based on regional gravity, seismic reflection and borehole data: how to explain a gravity maximum within a large sedimentary basin? *Journal of Geodynamics*, **47**, 142–152, https://doi.org/10.1016/j.jog.2008.07.004

Galeazzi, S., Point, O., Haddadi, N., Mather, J. and Druesne, D. 2010. Regional geology and petroleum systems of the Illizi–Berkine area of the Algerian Saharan platform: an overview. *Marine and Petroleum Geology*, **27**, 143–178, https://doi.org/10.1016/j.marpetgeo.2008.10.002

Genter, A., Castaing, C., Dezayes, C., Tenzer, H., Traineau, H. and Villemin, T. 1997. Comparative analysis of direct (core) and indirect (borehole imaging tools) collection of fracture data in the Hot Dry Rock Soultz reservoir (France). *Journal of Geophysical Research: Solid Earth*, **102**, 15 419–15 431, https://doi.org/10.1029/97JB00626

Geuzaine, C. and Remacle, J.F. 2009. Gmsh: a 3-D finite element mesh generator with built-in pre-and post-processing facilities. *International Journal for Numerical Methods in Engineering*, **79**, 1309–1331, https://doi.org/10.1002/nme.2579

Gharbi, M., Espurt, N. and Masrouhi, A. 2015. Style of Atlassic tectonic deformation and geodynamic evolution of the southern Tethyan margin, Tunisia. *Marine and Petroleum Geology*, **66**, 801–816, https://doi.org/10.1016/j.marpetgeo.2015.07.020

Gharsalli, R. and Bédir, M. 2020. Sequence stratigraphy of the subsurface cambro-ordovician siliciclastic deposits in the Chotts basin, Southern Tunisia: Petroleum implications. *Journal of African Earth Sciences*, **172**, 103997, https://doi.org/10.1016/j.jafrearsci.2020.103997

Grech, P. and Addala, K. 2014. Sabria Field – Unlocking reserves through understanding. Paper presented at the 4th Tunisian Oil and Gas Summit, 25–27 September 2014, Hamammet, Tunisia.

Grimm Lima, M.M., Schädle, P., Vogler, D., Saar, M.O. and Kong, X.Z. 2020. A numerical model for formation dry-out during $CO_2$ injection in fractured reservoirs using the MOOSE framework: implications for $CO_2$-based geothermal energy extraction. *In*: *Proceedings World Geothermal Congress 2020 Reykjavik, Iceland, 26 April–2 May 2020*. ETH Zurich, Zurich, Switzerland, 15024.

Gutierrez, M. and Youn, D.-J. 2015. Effects of fracture distribution and length scale on the equivalent continuum elastic compliance of fractured rock masses. *Journal of Rock Mechanics and Geotechnical Engineering*, **7**, 626–637, https://doi.org/10.1016/j.jrmge.2015.07.006

Gutmanis, J., i Oró, L.A., Díez-Canseco, D., Chebbihi, L., Awdal, A. and Cook, A. 2018. Fracture analysis of outcrop analogues to support modelling of the subseismic domain in carbonate reservoirs, south-central Pyrenees. *Geological Society, London, Special Publications*, **459**, 139–156, https://doi.org/10.1144/SP459.2

Healy, D., Rizzo, R.E. *et al.* 2017. FracPaQ: A MATLAB™ toolbox for the quantification of fracture patterns. *Journal of Structural Geology*, **95**, 1–16, https://doi.org/10.1016/j.jsg.2016.12.003

Hooker, J.N., Gomez, L.A., Laubach, S.E., Gale, J.F.W. and Marrett, R. 2012. Effects of diagenesis (cement precipitation) during fracture opening on fracture aperture-size scaling in carbonate rocks. *Geological Society, London, Special Publications*, **370**, 187–206, https://doi.org/10.1144/SP370.9

Hooker, J.N., Laubach, S.E. and Marrett, R. 2014. A universal power-law scaling exponent for fracture apertures in sandstones. *Geological Society of America Bulletin*, **126**, 1340–1362, https://doi.org/10.1130/B30945.1

Huang, N., Jiang, Y., Liu, R. and Li, B. 2017. Estimation of permeability of 3-D discrete fracture networks: an alternative possibility based on trace map analysis. *Engineering Geology*, **226**, 12–19, https://doi.org/10.1016/j.enggeo.2017.05.005

Jabir, A., Cerepi, A., Loisy, C. and Rubino, J.-L. 2020. Stratigraphy, sedimentology and paleogeography of a Palaeozoic succession, Ghadames and Jefarah basin, Libya and Tunisia. *Journal of African Earth Sciences*, **163**, 103642, https://doi.org/10.1016/j.jafrearsci.2019.103642

Jaglan, H., Qayyum, F. and Hélène, H. 2015. Unconventional seismic attributes for fracture characterization. *First Break*, **33**, 101–109, https://doi.org/10.3997/1365-2397.33.3.79520

Jing, L. and Stephansson, O. 2007. *Fundamentals of Discrete Element Methods for Rock Engineering: Theory and Applications*. Elsevier, Amsterdam.

Johns, R.A., Steude, J.S., Castanier, L.M. and Roberts, P.V. 1993. Nondestructive measurements of fracture aperture in crystalline rock cores using X ray computed tomography. *Journal of Geophysical Research: Solid Earth*, **98**, 1889–1900, https://doi.org/10.1029/92JB02298

Jung, A., Fenwick, D.H. and Caers, J. 2013. Training image-based scenario modeling of fractured reservoirs for flow uncertainty quantification. *Computational Geosciences*, **17**, 1015–1031, https://doi.org/10.1007/s10596-013-9372-0

Karatalov, N., Stefaniak, A. and Vaughan, L. 2017. DFN modeling aided reservoir characterization. Paper SPE-188641-MS presented at the Abu Dhabi International Petroleum Exhibition & Conference, 13–16 November 2017, Abu Dhabi, UAE.

Kattenhorn, S.A. and Pollard, D.D. 2001. Integrating 3-D seismic data, field analogs, and mechanical models in the analysis of segmented normal faults in the Wytch Farm oil field, southern England, United Kingdom. *AAPG Bulletin*, **85**, 1183–1210, https://doi.org/10.1306/8626CA91-173B-11D7-8645000102C1865D

Khoshbakht, F., Azizzadeh, M., Memarian, H., Nourozi, G.H. and Moallemi, S.A. 2012. Comparison of electrical image log with core in a fractured carbonate reservoir. *Journal of Petroleum Science and Engineering*, **86**, 289–296, https://doi.org/10.1016/j.petrol.2012.03.007

Kraouia, S., Mabrouk El Asmi, A., Ben Salem, A. and Saidi, M. 2019. Geopetroleum evaluation of the Ordovician and Triassic reservoirs in the southern part of Chotts area (Southern Tunisia) and maturity modeling. *In:* Banerjee, S., Barati, R. and Pati, S. (eds) *Advances in Petroleum Engineering and Petroleum Geochemistry: Proceedings of the 1st Springer Conference of the Arabian Journal of Geosciences (CAJG-1), Tunisia 2018*. Springer, Cham, Switzerland, 153–156, https://doi.org/10.1007/978-3-030-01578-7_36

Lamarche, J., Lavenu, A.P.C., Gauthier, B.D.M., Guglielmi, Y. and Jayet, O. 2012. Relationships between fracture patterns, geodynamics and mechanical stratigraphy in carbonates (South-East Basin, France). *Tectonophysics*, **581**, 231–245, https://doi.org/10.1016/j.tecto.2012.06.042

Laronne Ben-Itzhak, L., Aharonov, E., Karcz, Z., Kaduri, M. and Toussaint, R. 2014. Sedimentary stylolite networks and connectivity in limestone: large-scale field observations and implications for structure evolution. *Journal of Structural Geology*, **63**, 106–123, https://doi.org/10.1016/j.jsg.2014.02.010

Laubach, S.E. and Ward, M.E. 2006. Diagenesis in porosity evolution of opening-mode fractures, Middle Triassic to Lower Jurassic la Boca Formation, NE Mexico. *Tectonophysics*, **419**, 75–97, https://doi.org/10.1016/j.tecto.2006.03.020

Lavenu, A.R.C., Lamarche, J., Gallois, A. and Gauthier, B.D.M. 2013. Tectonic versus diagenetic origin of fractures in a naturally fractured carbonate reservoir analog (Nerthe anticline, southeastern France). *AAPG Bulletin*, **97**, 2207–2232, https://doi.org/10.1306/04041312225

Lavier, L.L. and Buck, W.R. 2002. Half graben versus large-offset low-angle normal fault: importance of keeping cool during normal faulting. *Journal of Geophysical Research: Solid Earth*, **107**, ETG 8-1–ETG 8-13, https://doi.org/10.1029/2001JB000513

Lazzez, M., Zouaghi, T. and Youssef, M.B. 2008. Austrian phase on the Northern African margin inferred from sequence stratigraphy and sedimentary records in southern Tunisia (Chotts and Djeffara areas). *Comptes Rendus Geoscience*, **340**, 543–552, https://doi.org/10.1016/j.crte.2008.05.005

Lei, Q., Latham, J.P. and Tsang, C.F. 2017. The use of discrete fracture networks for modelling coupled geomechanical and hydrological behaviour of fractured rocks. *Computers and Geotechnics*, **85**, 151–176, https://doi.org/10.1016/j.compgeo.2016.12.024

Lepillier, B., Daniilidis, A., Doonechaly Gholizadeh, N., Bruna, P.O., Kummerow, J. and Bruhn, D. 2019. A fracture flow permeability and stress dependency simulation applied to multi-reservoirs, multi-production scenarios analysis. *Geothermal Energy*, **7**, 24, https://doi.org/10.1186/s40517-019-0141-8

Li, J.Z., Laubach, S., Gale, J. and Marrett, R. 2018. Quantifying opening-mode fracture spatial organization in horizontal wellbore image logs, core and outcrop: Application to Upper Cretaceous Frontier Formation tight gas sandstones, USA. *Journal of Structural Geology*, **108**, 137–156, https://doi.org/10.1016/j.jsg.2017.07.005

Loza Espejel, R., Alves, T.M. and Blenkinsop, T.G. 2020. Multi-scale fracture network characterisation on carbonate platforms. *Journal of Structural Geology*, **140**, 104160, https://doi.org/10.1016/j.jsg.2020.104160

Maerten, L., Maerten, F., Lejri, M. and Gillespie, P. 2016. Geomechanical paleostress inversion using fracture data. *Journal of Structural Geology*, **89**, 197–213, https://doi.org/10.1016/j.jsg.2016.06.007

Manzocchi, T. 2002. The connectivity of two-dimensional networks of spatially correlated fractures. *Water Resources Research*, **38**, 1162, https://doi.org/10.1029/2000WR000180

Marrett, R., Ortega, O.J. and Kelsey, C.M. 1999. Extent of power-law scaling for natural fractures in rock. *Geology*, **27**, 799–802, https://doi.org/10.1130/0091-7613(1999)027<0799:EOPLSF>2.3.CO;2

Mathieu, G. 1949. *Contribution à L'étude des Monts Troglodytes dans l'Extrême-Sudtunisien: Géologie Régionale des Environs de Matmata Medenine et Foum-Tatahouine*. Annales des Mines et de la Geologie, **4**. Direction des Travaux Publics, Régence de Tunis, Protectorat Français.

Mauldon, M. and Dershowitz, W. 2000. A multi-dimensional system of fracture abundance measures. *Geological Society of America Abstracts with Programs*, **32**, 474.

Mejri, F., Burollet, P.F. and Ferjani, A.B. 2006. *Petroleum Geology of Tunisia: A Renewed Synthesis*. Enterprise Tunisienne d'Activités Pétrolières (ETAP), Tunis.

Micarelli, L., Benedicto, A. and Wibberley, C.A.J. 2006. Structural evolution and permeability of normal fault zones in highly porous carbonate rocks. *Journal of Structural Geology*, **28**, 1214–1227, https://doi.org/10.1016/j.jsg.2006.03.036

Michie, E.A.H., Haines, T.J., Healy, D., Neilson, J.E., Timms, N.E. and Wibberley, C.A.J. 2014. Influence of carbonate facies on fault zone architecture. *Journal of Structural Geology*, **65**, 82–99, https://doi.org/10.1016/j.jsg.2014.04.007

Mitchell, T.M. and Faulkner, D.R. 2009. The nature and origin of off-fault damage surrounding strike-slip fault zones with a wide range of displacements: A field study from the Atacama fault system, northern Chile. *Journal of Structural Geology*, **31**, 802–816, https://doi.org/10.1016/j.jsg.2009.05.002

Nelson, R.A. 2001. *Geologic Analysis of Naturally Fractured Reservoirs*. Gulf Professional Publishing, Houston, TX.

Olson, J.E. 2003. Sublinear scaling of fracture aperture versus length: an exception or the rule? *Journal of Geophysical Research: Solid Earth*, **108**, 2413, https://doi.org/10.1029/2001JB000419

Olson, J.E. and Schultz, R.A. 2011. Comment on 'A note on the scaling relations for opening mode fractures in rock' by CH Scholz. *Journal of Structural Geology*, **33**, 1523–1524, https://doi.org/10.1016/j.jsg.2011.07.004

Ortega, O.J., Marrett, R.A. and Laubach, S.E. 2006. A scale-independent approach to fracture intensity and average spacing measurement. *AAPG Bulletin*, **90**, 193–208, https://doi.org/10.1306/08250505059

Pan, D., Li, S., Xu, Z., Zhang, Y., Lin, P. and Li, H. 2019. A deterministic–stochastic identification and modelling method of discrete fracture networks using laser scanning: development and case study. *Engineering Geology*, **262**, 105310, https://doi.org/10.1016/j.enggeo.2019.105310

Permann, C.J., Gaston, D.R. *et al.* 2020. MOOSE: enabling massively parallel multiphysics simulation. *SoftwareX*, **11**, 100430, https://doi.org/10.1016/j.softx.2020.100430

Piazolo, S., Bons, P.D. *et al.* 2019. A review of numerical modelling of the dynamics of microstructural development in rocks and ice: Past, present and future. *Journal of Structural Geology*, **125**, 111–123, https://doi.org/10.1016/j.jsg.2018.05.025

Poulet, T., Paesold, M. and Veveakis, M. 2017. Multi-physics modelling of fault mechanics using REDBACK: a parallel open-source simulator for tightly coupled problems. *Rock Mechanics and Rock Engineering*, **50**, 733–749, https://doi.org/10.1007/s00603-016-0927-y

Poulet, T., Lesueur, M. and Kelka, U. 2021. Dynamic modelling of overprinted low-permeability fault cores and surrounding damage zones as lower dimensional interfaces for multiphysics simulations. *Computers & Geosciences*, **150**, 104719, https://doi.org/10.1016/j.cageo.2021.104719

Raulin, C., de Lamotte, D.F., Bouaziz, S., Khomsi, S., Mouchot, N., Ruiz, G. and Guillocheau, F. 2011. Late Triassic–early Jurassic block tilting along E–W faults, in southern Tunisia: New interpretation of the Tebaga of Medenine. *Journal of African Earth Sciences*, **61**, 94–104, https://doi.org/10.1016/j.jafrearsci.2011.05.007

Reeh, G., Boote, D. and Reston, T. 2019. Structural history of the Jefarrah Fault system, NW Libya. Presented at the PESGB HCS E&P Africa Conference, 1–2 October 2019, London, UK.

Richard, P.D., Bazalgette, L., Volery, C. and Toukhi, A. 2022. Scale discrepancy paradox between observation and modelling in fractured reservoir models in oil and gas industry. *Geological Magazine*, **159**, 1914–1935, https://doi.org/10.1017/S0016756822000620

Roskam, P.A. 2016. *Sub-Seismic Deformation in the Sabria Oilfield, Central Tunisia*. MSc thesis, Delft University of Technology, Delft, The Netherlands.

RPS Energy 2018. *Reserves & Contingent Resources Evaluation: Sabria, Chouech Es Saida, Ech Chouech, and Sanghar Fields, Tunisia*. Report No. CC01512 prepared for Serinus Energy Inc. RPS Energy Canada Ltd, Calgary, Alberta, Canada.

Saïd, A., Baby, P., Chardon, D. and Ouali, J. 2011. Structure, paleogeographic inheritance, and deformation history of the southern Atlas foreland fold and thrust belt of Tunisia. *Tectonics*, **30**, TC6004, https://doi.org/10.1029/2011TC002862

Sanderson, D.J. and Nixon, C.W. 2015. The use of topology in fracture network characterization. *Journal of Structural Geology*, **72**, 55–66, https://doi.org/10.1016/j.jsg.2015.01.005

Serinus Energy 2022. *Corporate Presentation November 2022*. Serinus Energy plc.

Smith, R.Y. 2020. *Regional Geology and Fracture Network Characterisation of the Southern Chotts and Jeffara Basins, Central Tunisia*. MSc thesis, Delft University of Technology, Delft, The Netherlands.

Smith, R.Y., Lesueur, M., Kelka, U., Poulet, T. and Koehn, D. 2022. Using fractured outcrops to calculate permeability tensors: implications for geothermal fluid flow and the influence of seismic-scale faults. *Geological Magazine*, **159**, 2262–2278, https://doi.org/10.1017/S0016756822000309

Snow, D.T. 1969. Anisotropy permeability of fractured media. *Water Resources Research*, **5**, 1273–1289, https://doi.org/10.1029/WR005i006p01273

Soua, M. 2014. Paleozoic oil/gas shale reservoirs in southern Tunisia: An overview. *Journal of African Earth Sciences*, **100**, 450–492, https://doi.org/10.1016/j.jafrearsci.2014.07.009

Soumaya, A., Kadri, A., Ayed, N.B., Kim, Y.S., Dooley, T.P., Rajabi, M. and Braham, A. 2020. Deformation styles related to intraplate strike-slip fault systems of the Saharan–Tunisian Southern Atlas (North Africa): New kinematic models. *Journal of Structural Geology*, **140**, 104175, https://doi.org/10.1016/j.jsg.2020.104175

Stampfli, G.M. and Borel, G. 2002. A plate tectonic model for the Paleozoic and Mesozoic constrained by dynamic plate boundaries and restored synthetic oceanic isochrons. *Earth and Planetary Science Letters*, **196**, 17–33, https://doi.org/10.1016/S0012-821X(01)00588-X

Stephenson, B.J., Koopman, A., Hillgartner, H., McQuillan, H., Bourne, S., Noad, J.J. and Rawnsley, K. 2007. Structural and stratigraphic controls on fold-related fracturing in the Zagros Mountains, Iran: implications for reservoir development. *Geological Society, London, Special Publications*, **270**, 1–21, https://doi.org/10.1144/GSL.SP.2007.270.01.01

Stoll, M., Huber, F.M. *et al.* 2019. Experimental and numerical investigations on the effect of fracture geometry and fracture aperture distribution on flow and solute transport in natural fractures. *Journal of Contaminant Hydrology*, **221**, 82–97, https://doi.org/10.1016/j.jconhyd.2018.11.008

Swanson, M.T. 1988. Pseudotachylyte-bearing strike-slip duplex structures in the Fort Foster Brittle Zone, S. Maine. *Journal of Structural Geology*, **10**, 813–828, https://doi.org/10.1016/0191-8141(88)90097-1

Tavani, S., Mencos, J., Bausà, J. and Muñoz, J.A. 2011. The fracture pattern of the Sant Corneli Bóixols oblique inversion anticline (Spanish Pyrenees). *Journal of Structural Geology*, **33**, 1662–1680, https://doi.org/10.1016/j.jsg.2011.08.007

Terzaghi, R.D. 1965. Sources of error in joint surveys. *Geotechnique*, **15**, 287–304, https://doi.org/10.1680/geot.1965.15.3.287

Toublanc, A., Renaud, S., Sylte, J.E., Clausen, C.K., Eiben, T. and Nådland, G. 2005. Ekofisk Field: fracture permeability evaluation and implementation in the flow model. *Petroleum Geoscience*, **11**, 321–330, https://doi.org/10.1144/1354-079304-622

Troudi, H., Chevalier, F. and Alouani, W. 2018. Insight on the exploration potential of the Ordovician gas play in Tunisia Ghadames Basin, North Africa. Paper SPE-192634-MSpresented at the Abu Dhabi International Petroleum Exhibition & Conference, 12–15 November 2018, Abu Dhabi, UAE, https://doi.org/10.2118/192634-MS

Walsh, J.J. and Watterson, J. 1988. Analysis of the relationship between displacements and dimensions of faults. *Journal of Structural Geology*, **10**, 239–247, https://doi.org/10.1016/0191-8141(88)90057-0

Watkins, H., Healy, D., Bond, C.E. and Butler, R.W. 2018. Implications of heterogeneous fracture distribution on reservoir quality; an analogue from the Torridon Group sandstone, Moine Thrust Belt, NW Scotland. *Journal of Structural Geology*, **108**, 180–197, https://doi.org/10.1016/j.jsg.2017.06.002

Welch, M.J., Souque, C., Davies, R.K. and Knipe, R.J. 2015. Using mechanical models to investigate the controls on fracture geometry and distribution in chalk. *Geological Society, London, Special Publications*, **406**, 281–309, https://doi.org/10.1144/SP406.5

Whitehead, W.S., Hunt, E.R. and Holditch, S.A. 1987. The effects of lithology and reservoir pressure on the in-situ stresses in the Waskom (Travis Peak) Field. Paper SPE-16403-MS presented at the SPE/DOE Joint Symposium on Low Permeability Reservoirs, 18–19 May 1987, Denver, Colorado, USA, https://doi.org/10.2118/16403-MS

Witherspoon, P.A., Wang, J.S., Iwai, K. and Gale, J.E. 1980. Validity of cubic law for fluid flow in a deformable rock fracture. *Water Resources Research*, **16**, 1016–1024, https://doi.org/10.1029/WR016i006p01016

Wu, H. and Pollard, D.D. 2002. Imaging 3-D fracture networks around boreholes. *AAPG Bulletin*, **86**, 593–604, https://doi.org/10.1306/61EEDB52-173E-11D7-8645000102C1865D

Zaafouri, A., Haddad, S. and Mannaî-Tayech, B. 2017. Subsurface Permian reef complexes of southern Tunisia: Shelf carbonate setting and paleogeographic implications. *Journal of African Earth Sciences*, **129**, 944–959, https://doi.org/10.1016/j.jafrearsci.2017.02.032

Zahn, C.K. and Hennings, P.H. 2009. Complex fracture development related to stratigraphic architecture: Challenges for structural deformation prediction, Tensleep Sandstone at the Alcova anticline, Wyoming. *AAPG Bulletin*, **93**, 1427–1446, https://doi.org/10.1306/08040909110

Zhang, L., Kang, Q., Chen, L. and Yao, J. 2016. Simulation of flow in multi-scale porous media using the lattice Boltzmann method on quadtree grids. *Communications in Computational Physics*, **19**, 998–1014, https://doi.org/10.4208/cicp.110315.190815a

Zouari, H., Kamoun, Y. and Regaya, K. 1987. *Carte Géologique au 1/100 000 de Matmata. Feuille No. 91*. Centre des Sciences de la Terre (INRST) and National Office of Mines (ONM), Tunis.